Research article

JHEP|Reports

O-GlcNAc transferase acts as a critical nutritional node for the control of liver homeostasis

Paula Ortega-Prieto,[1,†] Lucia Parlati,[1,†] Fadila Benhamed,[1] Marion Regnier,[1] Isadora Cavalcante,[2] Mélanie Montabord,[1] Rachel Onifarasoaniaina,[3] Maryline Favier,[3] Natasa Pavlovic,[4] Julie Magusto,[5] Michèle Cauzac,[1] Patrick Pagesy,[1] Jérémie Gautheron,[5] Chantal Desdouets,[4] Sandra Guilmeau,[1] Tarik Issad,[1,*] Catherine Postic[1,*]

[1]*Université Paris Cité, Institut Cochin, CNRS, INSERM, Paris, France;* [2]*Team Genomics and signaling of endocrine tumors, Institut Cochin, CNRS, INSERM, Université Paris Cité, Paris, France;* [3]*HistIM Platform, Institut Cochin, CNRS, INSERM, Université de Paris Cité, Paris, France;* [4]*Team Proliferation, Stress and Liver Physiopathology, Centre de Recherche des Cordeliers, INSERM, Sorbonne Université, Université Paris Cité, Paris, France;* [5]*Centre de Recherche Saint-Antoine, Sorbonne Université, Inserm, Paris, France*

JHEP Reports **2024.** https://doi.org/10.1016/j.jhepr.2023.100878

Background & Aims: *O*-GlcNAcylation is a reversible post-translational modification controlled by the activity of two enzymes, *O*-GlcNAc transferase (OGT) and *O*-GlcNAcase (OGA). In the liver, *O*-GlcNAcylation has emerged as an important regulatory mechanism underlying normal liver physiology and metabolic disease.
Methods: To address whether OGT acts as a critical hepatic nutritional node, mice with a constitutive hepatocyte-specific deletion of OGT (OGT^{LKO}) were generated and challenged with different carbohydrate- and lipid-containing diets.
Results: Analyses of 4-week-old OGT^{LKO} mice revealed significant oxidative and endoplasmic reticulum stress, and DNA damage, together with inflammation and fibrosis, in the liver. Susceptibility to oxidative and endoplasmic reticulum stress-induced apoptosis was also elevated in OGT^{LKO} hepatocytes. Although OGT expression was partially recovered in the liver of 8-week-old OGT^{LKO} mice, hepatic injury and fibrosis were not rescued but rather worsened with time. Interestingly, weaning of OGT^{LKO} mice on a ketogenic diet (low carbohydrate, high fat) fully prevented the hepatic alterations induced by OGT deletion, indicating that reduced carbohydrate intake protects an OGT-deficient liver.
Conclusions: These findings pinpoint OGT as a key mediator of hepatocyte homeostasis and survival upon carbohydrate intake and validate OGT^{LKO} mice as a valuable model for assessing therapeutical approaches of advanced liver fibrosis.
Impact and Implications: Our study shows that hepatocyte-specific deletion of *O*-GlcNAc transferase (OGT) leads to severe liver injury, reinforcing the importance of *O*-GlcNAcylation and OGT for hepatocyte homeostasis and survival. Our study also validates the *Ogt* liver-deficient mouse as a valuable model for the study of advanced liver fibrosis. Importantly, as the severe hepatic fibrosis of *Ogt* liver-deficient mice could be fully prevented upon feeding on a ketogenic diet (*i.e.* very-low-carbohydrate, high-fat diet) this work underlines the potential interest of nutritional intervention as antifibrogenic strategies.

Introduction

O-GlcNAcylation is a dynamic and reversible post-translational modification controlled by the activity of two enzymes, *O*-GlcNAc transferase (OGT) and *O*-GlcNAcase (OGA). OGT and OGA mediate the dynamic cycling of *O*-GlcNAcylation on a wide variety of cytosolic, nuclear, and mitochondrial proteins, in response to environmental changes, such as nutrients or stress challenges.[1] Therefore, *O*-GlcNAcylation has been proposed as a nutrient and stress sensor that mediates cellular adaptations ranging from transcription and translation to signal transduction and metabolism. As a result, disruption of *O*-GlcNAc homeostasis has been implicated in the pathogenesis of several human diseases, including cancer, diabetes, and neurodegeneration.[2]

In the liver, *O*-GlcNAcylation has emerged as an important regulatory mechanism underlying normal liver physiology and metabolic disease. *O*-GlcNAcylation significantly contributes to liver gluco-lipotoxicity by modulating key effectors of hepatic metabolism.[3,4] Moreover, OGT acts as a suppressor of hepatocyte necroptosis (a specific form of regulated cell death), and its hepatic deletion triggers liver fibrosis in mice.[5] Altogether, these studies suggested that OGT may act as a critical molecular switch between hepatocyte survival and death in response to chronic liver injury.[5]

Although several cellular functions of *O*-GlcNAcylation are clearly emerging, we hypothesise that OGT loss of function may prevent liver cells to cope with the oxidative stress induced by dietary glucose.[6–9] Indeed, OGT was shown to protect against oxidative stress by promoting antioxidant responses, whereas

Keywords: OGT; Oxidative stress; Liver fibrosis; Carbohydrate intake; Ketogenic diet.
Received 8 November 2022; received in revised form 6 July 2023; accepted 24 July 2023; available online 12 August 2023
† These authors contributed equally.
* Corresponding authors. Address: Institut Cochin, Inserm U101624, Rue du Faubourg Saint Jacques 75014 Paris, France. Tel.: +33 685849052 (C. Postic); +33 1 44412567 (T. Issad).
E-mail addresses: catherine.postic@inserm.fr (C. Postic), tarik.issad@inserm.fr (T. Issad).

lack of OGT correlates with high oxidative stress in response to elevated glucose concentrations.[10] To test this hypothesis, we first examined at different time points ranging from 2 weeks to 1 year the phenotype of mice with a constitutive OGT deficiency in hepatocytes (OGT^{LKO}) and fed a 70% carbohydrate diet. We then explored whether limiting carbohydrate intake at weaning could protect the liver against lack of OGT. Interestingly, analysis of OGT^{LKO} mice at 4 weeks revealed the onset of hepatic oxidative and endoplasmic reticulum (ER) stress, and DNA damage, together with liver inflammation and moderate fibrosis. Liver injury and fibrosis worsened with time when OGT^{LKO} mice were maintained on a high-carbohydrate diet, as characterised by advanced hepatic fibrosis and septa surrounding regenerative nodules. Interestingly, weaning OGT^{LKO} mice on a ketogenic low-carbohydrate, high-fat diet, to limit carbohydrate intake, fully prevented the severe hepatic alterations induced by early OGT deletion, including advanced fibrosis. These findings underline the critical role of OGT in hepatocyte homeostasis and survival upon carbohydrate intake. Our study also establishes the OGT^{LKO} mouse model as a spontaneous model of advanced fibrosis that may, in the future, facilitate therapeutic target identification for prevention and treatment of chronic liver disease.

Materials and methods

Generation of OGT^{LKO} mice

Conditional hepatic-specific OGT knockout mice (OGT^{LKO}) and control floxed littermates (OGT^{LWT}) were generated by crossing *Albumin-Cre; Ogt$^{F/Y}$* with *Ogt$^{F/F}$* mice. The *Ogt* locus was floxed on either side of exons 6–7 encoding amino acids 206 and 232. *Ogt* mice were obtained from Jackson Laboratories (JAX stock #00486).

Animals and nutritional challenges

All animal procedures were carried out according to the French guidelines for the care and use of experimental animals (animal authorisation agreements #9723, #19226, and #33226 from the University of Paris Ethical Committee, Paris, France). Mice (males and females) were housed in colony housing on a 12-h light/dark cycle. All mice were given free access to water and control chow diet (standard diet [SD] in % of calories: 69% of carbohydrates, 4% of fat, and 26% of proteins; SAFE #A03). Regarding nutritional challenges, OGT^{LWT} and OGT^{LKO} mice were weaned and fed for 5 weeks with a low-carbohydrate, high-fat (LCHF) diet (in percentage of calories: 21% of carbohydrates, 60% of fat, 19% of proteins) (SSNIF #E15742) or a ketogenic diet (KD in % of calories: 1% of carbohydrates, 94% of fat, 5% of proteins) (SSNIF #E15149). The age and sex of the mice are specified in the results and figure legends.

Blood glucose concentrations and glucose homeostasis

Blood glucose was measured in total blood using an Accu-Check glucometer (Roche). Glucose tolerance tests, pyruvate tolerance tests, and insulin tolerance tests were performed in 4-week-old OGT^{LKO} and control OGT^{LWT} littermates. For glucose tolerance tests, mice were fasted 4–5 h and received 2 g/kg of glucose; for pyruvate tolerance tests, mice were fasted overnight and received 1 g/kg of pyruvate; and for insulin tolerance tests, mice were fasted 4–5 h and received 0.75 U/kg of insulin. Blood glucose concentrations were measured over a period of 120 min for all tests.

β-Hydroxybutyrate concentrations

β-Hydroxybutyrate was measured using Optium β-Ketone test strips that carried Optium Xceed sensors (Abbott Diabetes Care).

Cytokines and liver enzymes concentrations

Concentrations of serum cytokines were analysed using the V-PLEX Proinflammatory Panel 1 Mouse Kit (Meso Scale, K15048D). Serum alanine aminotransferase (ALT), aspartate aminotransferase (AST), lactate dehydrogenase (LDH), alkaline phosphatase (ALP), and total and direct bilirubin concentrations were determined using an automated Monarch device (Laboratoire de Biochimie, Faculté de Médecine Bichat, Paris, France).

RNA isolation, reverse transcription, and qPCR

Snap-frozen liver tissue was powdered, and approximately 15 mg of liver powder was used for RNA extraction using the SV Total RNA Isolation System (Promega, Madison, WI, USA; Z3101). mRNAs were reverse transcribed, and cDNA levels were measured by quantitative PCR (qPCR) (LightCycler480 SYBR Green I Master, Roche) using the primers described in Table S4. Gene expression was normalised over expression of the TATA-box binding protein (TBP) mRNA levels.

Protein extraction, Western blot, and WGA precipitation experiments

Whole tissue was lysed in lysis buffer (20 mM Tris HCl [pH 7.5], 150 mM NaCl, 5 mM EDTA, 50 mM NaF, 30 mM NaP, 1% Triton X-100, EDTA-free protease inhibitor cocktail [Roche, 4693132001], orthovanadate 1 mM, Thiamet-G 10 μM [Sigma, SML0244]). Western blot was performed using 30 μg of lysate. For lectin-based precipitation assay, the lysate (1 mg of proteins) was incubated overnight with 25 μl of wheat germ agglutinin (WGA) agarose beads (Sigma, L1882) at 4 °C. The precipitate was resolved by SDS-PAGE and immunoblotted with specific antibodies. Antibodies used are the following: anti-OGT (Sigma, SAB4200311), anti-*O*-GlcNAc antibody (RL2, ab2739), anti-glyceraldehyde 3-phosphate dehydrogenase (GAPDH) (Santa Cruz, sc-25778), anti-β-actin (CST #4970), anti-cyclin A2 (CycA2) (Santa Cruz, sc-596), anti-cyclin D1 (CycD1) (CST #2978), anti-proliferating cell nuclear antigen (PCNA) (CST #2586), anti-p62 (Enzo Life Sciences, BML-PW9860-0100), anti-p-p62 (CST #14354), anti-CCAAT–enhancer-binding protein homologous protein (CHOP) (CST #5554), anti-γH2AX (CST #2577), anti-H2AX total (CST #7631), anti-cleaved caspase-3 (CST #9661), anti-mixed lineage kinase domain-like pseudokinase (MLKL) (ab172868), anti-receptor-interacting serine/threonine-protein kinase 3 (RIPK3) (orb74415), anti-forkhead box protein o1 (Foxo1) (CST #2880), anti-c-Jun N-terminal kinase (JNK) (CST #9252), and anti-p-JNK (CST #9255). Semiquantitative analysis was performed using ChemiDoc software (Bio-Rad).

Histological analyses and tissue staining

Fixed livers (4% paraformaldehyde, 24 h at 4 °C) were embedded in paraffin and sliced at 7 μm. After deparaffinisation and rehydration, slides were stained with H&E, Sirius Red, and alpha-smooth muscle actin (αSMA) for fibrosis detection. In the case of immunolabelling, antigen retrieval was performed in citrate buffer for 10 min at 95 °C and treated with peroxidase blocking reagent (Sigma, H1009). Slides were permeabilised with 0.01% Tween20, and unspecific antigenicity was blocked with 2% bovine serum albumin and 2% serum, from the species in which the secondary antibody was raised. Primary antibodies used are the following: anti-OGT (Abcam, ab96718), anti-Ki67 (Thermo

Fisher, MA5-14520), anti-hepatocyte nuclear factor 4 alpha (HNF4α) (Santa Cruz, sc-6556), anti-sex-determining region Y-box 2 (SOX9) (EMD Millipore, ab5535), anti-cytokeratin 19 (Krt19) (Abcam, ab52625), anti-F4/80 (CST#70076), and anti-malondialdehyde (MDA) (Abcam, ab27642). HRP-conjugated secondary antibodies were revealed by incubation with DAB substrate (Dako, K3468), co-stained with haematoxylin (Vector Laboratories, H-3404), and mounted with VectaMount™ mounting medium (Vector Laboratories, H-5000). For apoptosis, the terminal deoxynucleotidyl transferase dUTP nick end labelling (TUNEL) kit (EMD Millipore kit S71000) was used. Analysis of images was processed using QuPath software.

Polyploidy assessment

To analyse polyploidy, liver sections were stained with Hoechst 33342, after which a dataset with nuclei size and circularity was extracted using QuPath. Then, by using R software (R Foundation for Statistical Computing, Vienna, Austria), a dataset containing only hepatocyte nuclei was generated based on size (>30 μm) and circularity (>0.8). Nuclear ploidy was assessed automatically, by a specific macro developed using Image J software, as previously described.[11] Hepatocyte polyploidy is presented as the ratio between the number of polyploid cells and total hepatocytes.

Liver neutral lipid analysis

Hepatic lipids were extracted from liver samples as previously described elsewhere.[12] Briefly, 50 mg of liver was homogenised in 2:1 (v/v) methanol/ethylene glycol tetraacetic acid (5 mM), and lipids from 2 mg of liver were extracted in a mix of methanol, chloroform, and water (2.5:2.5:2, v/v/v) in the presence of internal standards (glyceryltrinonadecanoate, stigmasterol, and cholesteryl heptadecanoate). Triglycerides, free cholesterol, and cholesterol esters were analysed by gas chromatography on a Focus Thermo Electron system using a Zebron-1 Phenomenex fused-silica capillary column (5 m, 0.32 mm inner diameter, 0.50-μm film thickness). The oven temperature was programmed from 200 to 350 °C at a rate of 5 °C/min, and the carrier gas was hydrogen (0.5 bar). The injector and detector were at 315 and 345 °C, respectively.

Liver fatty acid analysis

Fatty acid methyl esters (FAME) molecular species were extracted from an equivalent of 1 mg liver tissue in the presence of internal standards glyceryl triheptadecanoate (2 μg). The lipid extract was transmethylated with 1 ml boron trifluoride in methanol (14% solution; Sigma) and 1 ml heptane for 60 min at 80 °C and evaporated to dryness. The FAMEs were extracted with heptane/water (2:1). The organic phase was evaporated to dryness and dissolved in 50 μl ethyl acetate. A sample (1 μl) of total FAMEs was analysed with gas–liquid chromatography (Clarus 600 Perkin Elmer system, with Famewax RESTEK fused-silica capillary columns, 30-m × 0.32-mm inner diameter, 0.25-μm film thickness). Oven temperature was programmed to increase from 110 to 220 °C at a rate of 2 °C/min, and the carrier gas was hydrogen (7.25 psi). Injector and detector temperatures were 225 and 245 °C, respectively.

Liver sphingomyelin and ceramide analysis

Lipids were extracted from the liver (1 mg) as described by Bligh and Dyer[12] in dichloromethane/methanol (2% acetic acid)/water (2.5:2.5:2, v/v/v). Internal standards were added (ceramide [Cer] d18:1/15:0, 16 ng; sphingomyelin [SM] d18:1/12:0, 16 ng). The solution was centrifuged at 458 ×*g* for 3 min. The organic phase was collected and dried under azote and then dissolved in 50 μl MeOH. Sample solutions were analysed using an Agilent 1290 UPLC system coupled to a G6460 triple quadripole spectrometer (Agilent Technologies). MassHunter software was used for data acquisition and analysis. A Kinetex HILIC column was used for liquid chromatography separations. The column temperature was maintained at 40 °C. Mobile phase A was acetonitrile, and B was 10 mM ammonium formate in water at pH 3.2. The gradient was as follows: from 10 to 30% B in 10 min; 100% B from 10 to 12 min; and then back to 10% B at 13 min for 1 min to re-equilibrate before the next injection. The flow rate of the mobile phase was 0.3 ml/min, and the injection volume was 5 μl. An electrospray source was used in positive ion mode. The collision gas was nitrogen. Needle voltage was set at +4,000 V. Several scan modes were used. First, to obtain the naturally different masses of different species, we analysed cell lipid extracts with a precursor ion scan at 184 and 264 *m*/*z* for SM and Cer, respectively. The collision energy optimums for Cer and SM were 25 and 45 eV, respectively. Then, the corresponding standard reference material transitions were used to quantify different phospholipid species for each class. Two 9 multiple-reaction monitoring acquisitions were necessary, owing to important differences between phospholipid classes. Data were treated with QqQ Quantitative (vB.05.00) and Qualitative Analysis software (vB.04.00).

Microarray based transcriptome profiling

Liver RNA extraction was performed as mentioned previously and checked for integrity using Bioanalyzer. Microarray experiment and data normalisation were performed at the transcriptomic core facility at Cochin Institute. Briefly, gene expression profiling was carried out on five biological replicates per condition. After RNA quality validation with Bioanalyzer 2100, RNA was reversed transcribed following the manufacturer protocol (GeneChip® WT Plus Reagent Kit, Thermo Fisher). After fragmentation and biotin labelling, cDNA was hybridised to GeneChip® Clariom S Mouse (Thermo Fisher) and scanned using the GCS3000 7G. The images were analysed with Expression Console software (Thermo Fisher). Raw data were normalised using the robust multichip algorithm (RMA). Statistics and RMA normalisation were performed using TAC4.0 software (Thermo Fisher).

Downstream analysis was done to identify differentially expressed (DE) genes based on comparison with control conditions. The DE genes were selected based on the corrected *p* value for false discovery rate (FDR *p* value <0.05) and the fold change from OGT^{LKO} mice compared with controls (upregulated genes: fold change ≥2; downregulated genes: fold change ≤-2). A Venn diagram was performed using the interactive tool 'Venny 2.1.0'.[13] Upregulated and downregulated genes were annotated using Reactome gene set. Functional enrichment of specific pathways in the gene set was performed using Fisher's exact test and FDR correction. Pathways were considered significantly enriched at a FDR <0.05. R version 3.6.2 (R Foundation for Statistical Analysis) and R packages were used for bioinformatic analysis and graph representation. Volcano plots were represented using the 'Enhanced Volcano' package.[14] Heatmaps were represented using 'pheatmap' package,[15] where correlation clustering distance row was applied.

Primary hepatocyte isolation and culture

Four-week-old mice were anaesthetised with a 10:1 ketamine–xylazine solution intra-peritoneally. Liver was perfused through the portal vein with HBSS followed by collagenase perfusion. Cell viability was calculated by the trypan blue exclusion test using a Malassez chamber and seeded in six-well plates at a concentration of 500,000 cells per well. Cells were seeded in medium M199 5 mM of glucose (Thermo Fisher, #11150059) supplemented with 100 μg/ml streptomycin, 100 U/ml of penicillin, L-glutamine (2 mM), 0.1% bovine serum albumin, 2.5% Nu-Serum (BD Bioscience, Cat#355104), and dexamethasone (100 nM, Novo Nordisk). For reduced glutathione/oxidised glutathione (GSH/GSSG) assay, hepatocytes were seeded in 96-well plates at a concentration of 15,000 cells per well. Twenty-four hours after seeding, the GSH/GSSG ratio was measured using the GSH/GSSG-Glo assay kit (Promega) in accordance with the manufacturer's instructions. Experiments with staurosporine (StS) were performed by seeding hepatocytes in 6-cm^2 dishes at a concentration of 1.5 × 10^6 cells per dish. Twenty-four hours after seeding, cells were treated with 10 μM of StS (Sigma, S4400) and harvested 0, 2, 4, and 8 h after treatment for protein extraction. For thapsigargin experiments, 24 h after seeding, cells were treated with 0.3 μM of thapsigargin (Sigma, T9033) for 24 h. The total level of lipid peroxidation was analysed by flow cytometry-based BODIPY 581/591 assays (Molecular Probes), as recommended by the manufacturer. Forty-eight hours after seeding, cells were treated with 5 μM of BODIPY for 30 min at 37 °C. Cells were then collected and washed with PBS. For each experiment, 20,000 events were acquired by flow cytometry using a NovoCyte cytometer (Ozyme). Data were analysed using the NovoExpress software. Total reactive oxygen species (ROS) levels were measured by using the CellROX Deep Red reagent (Thermo Fisher) at a final concentration of 2.5 μM and then incubated for 30 min at 37 °C. Data were analysed using the NovoExpress software. For antioxidant response element (ARE) luciferase activity, cells were transfected with a 3 × ARE luciferase reporter[16] and a β-galactosidase plasmid using Lipofectamine 2000 and Opti-MEM media. After overnight incubation, medium was changed to low glucose (5 mM) for 24 h. Luciferase assay was performed after cell lysis. β-Galactosidase assays were performed for normalisation of 3 × ARE luciferase activity.

SHG microscopy for fibrosis quantification

Second harmonic generation (SHG) images were acquired using a multiphoton Leica DIVE microscope (Leica Microsystems GmbH, Wetzlar, Germany) coupled with a Coherent Discovery (Coherent Inc., Santa Clara, CA, USA) laser source. Five fields of view were acquired from paraffin-embedded 7-μm-thick sections of liver. Two-photon-excited autofluorescence and SHG images were acquired through a Leica Microsystems HCX IRAPO 25 × /0.95 water immersion objective by tuning the laser at 1,040 nm at constant power, and photomultiplier tubes and hybrid detectors were used at constant 800 V and 80% gain, respectively, allowing direct comparison of SHG intensity values. Circularly polarised laser pulse was sent to the microscope objective to excite isotropically the slice regardless of the orientation of fibrillar collagen. To quantify SHG, the microscope was calibrated using a non-fibrotic control liver section. SHG score was proceeded using a home-made ImageJ (http://imagej.nih.gov/ij/) routine, as described previously.[17]

Statistical analysis

All statistical analysis were performed using Prism (GraphPad Software Inc.F, San Diego, CA, USA). The number of independent experiments performed and the statistical test used are indicated in each figure legend. To compare two groups, unpaired student *t* test (Mann –Whitney *U* test) was used, while for 2 and additional groups, two-way Anova followed by Bonferroni *post hoc* test was used.

Results

Hepatocyte-specific OGT deletion triggers liver inflammation and moderate fibrosis at 4 weeks

Four weeks after birth, fed blood glucose, body weight, liver and spleen weight were not found different in OGT^{LKO} mice compared with OGT^{LWT} mice (Fig. 1A). OGT mRNA and protein levels (assessed by Western blot and immunostaining) were significantly reduced only in the liver of OGT^{LKO} mice, together with a parallel decrease in *O*-GlcNAcylated proteins (Fig. 1B, D, and E), confirming recombination efficiency and tissue specificity. We also observed a significant decrease in OGA expression in the liver (Fig. 1C). The activities of OGT and OGA are governed by multi-layered feedback mechanisms that finely tune the overall levels of *O*-GlcNAcylation in the cell. Studies have established that alterations in OGA activity affect OGT activity and vice versa.[18] Although the mechanisms used to modulate OGA protein levels in response to *O*-GlcNAc remain unknown, studies have suggested that OGA transcription is sensitive to changes in *O*-GlcNAc homeostasis and is potentially regulated by *O*-GlcNAc.[18] Further analysis revealed decreased blood concentrations upon short-term fasting (5 h) (Fig. S1A), improved glucose (Fig. S1B), and pyruvate tolerance (Fig. S1C) in OGT^{LKO} mice compared with OGT^{LWT} mice, without, however, any modification in insulin sensitivity (Fig. S1D). Decreased fasting blood glucose and increased pyruvate tolerance suggested decreased gluconeogenic capacity in OGT^{LKO} mice compared with OGT^{LWT} mice. To better understand the improvement in glucose homeostasis observed in OGT^{LKO} mice, we measured protein and *O*-GlcNAcylation levels[4] of the transcription factor Foxo1 (Fig. S1E), which is known to stimulate the expression of gluconeogenic genes, including glucose-6-phosphatase (*G6Pase*) and phosphoenolpyruvate carboxykinase (*Pepck*) (Fig. S1F). Of note, Foxo1 *O*-GlcNAcylation levels were markedly decreased in the liver of OGT^{LKO} mice compared with OGT^{LWT} mice (Fig. S1E), as well as mRNA levels of its target genes (*G6Pase* and *Pepck*) (Fig. S1F). Histological assessment by H&E, Sirius Red, or αSMA staining evidenced hepatic parenchymal alteration in OGT^{LKO} mice compared with OGT^{LWT} mice. In fact, OGT^{LKO} livers showed hepatocellular ballooning and moderate fibrosis together with fibroblast activation (Fig. 1E). In agreement, the expression of fibrosis markers (transforming growth factor beta [*Tgfβ*], *αSma*, collagen type III alpha 1 chain [*Col3a1*], and collagen type VI alpha 1 chain [*Col6a1*]) was found significantly increased in livers of OGT^{LKO} mice compared with OGT^{LWT} mice (Fig. 1F). In addition, positive staining for TUNEL, cytokeratin 7 (Krt7), and SOX9 in livers of 4-week-old OGT^{LKO} mice suggested emerging liver injury and apoptosis, ductular reaction, and hepatic progenitor cell activation (Fig. 1E). This observation was correlated with a significant increase in ALT in OGT^{LKO} mice, whereas two other markers of liver injury (AST and LDH) were not found statistically different

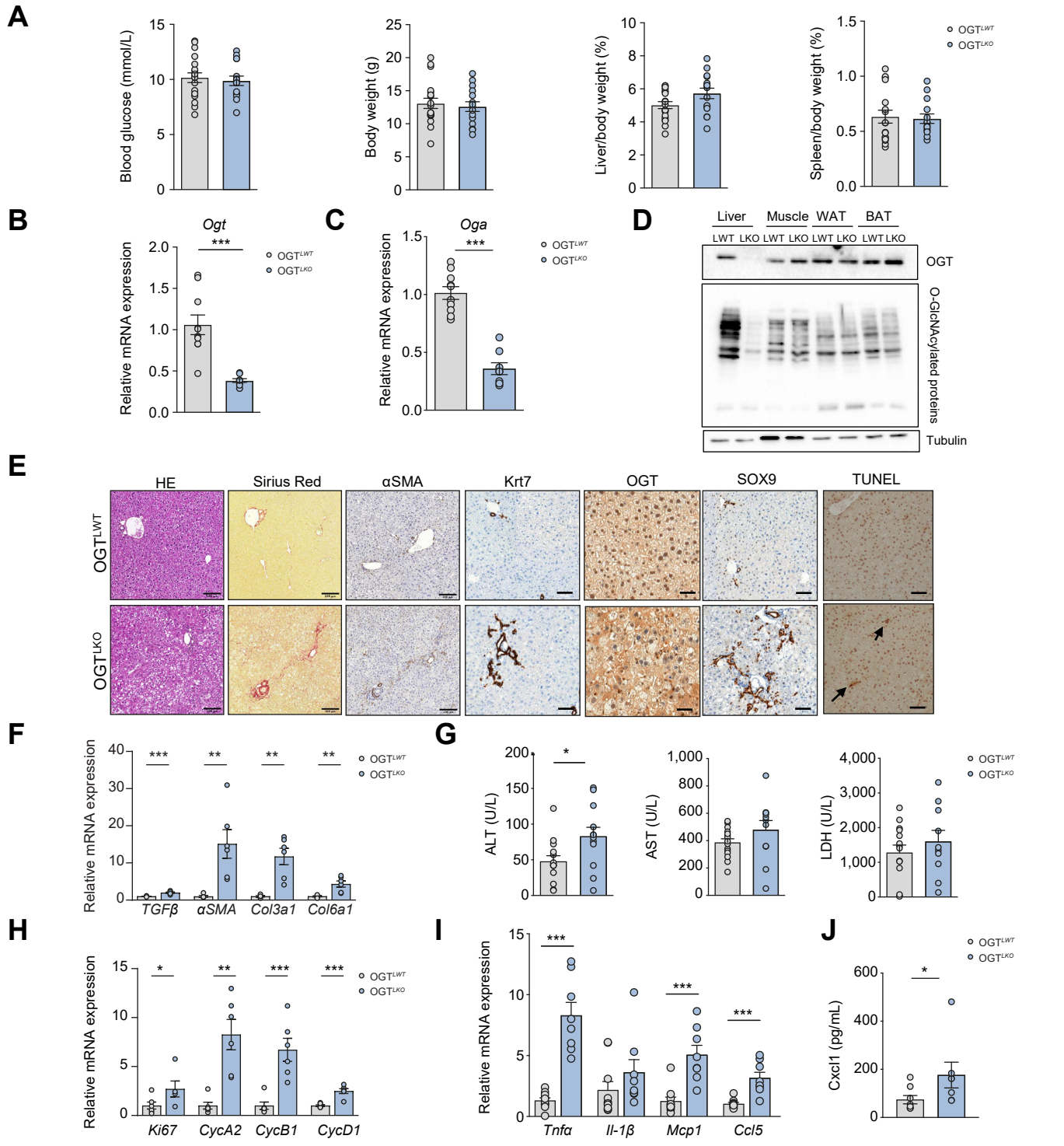

Fig. 1. Hepatocyte-specific OGT deletion leads to liver inflammation and moderate liver injury at 4 weeks. Male liver-specific *Ogt* knockout mice (OGT^{LKO}) and control floxed littermates (OGT^{LWT}) were studied 4 weeks after birth in the fed state. (A) Fed blood glucose (mmol/L), body weight (g), liver weight, and spleen weight are shown. Liver and spleen weights are represented as percentage of body weight. (B) Relative *Ogt* expression normalised to TBP. (C) Relative *Oga* expression normalised to TBP. (D) Western blot analysis of OGT and *O*-GlcNAcylation levels in the liver, muscle, WAT, and BAT of OGT^{LWT} and OGT^{LKO} mice. Tubulin was used as a loading control. One representative sample is presented per condition. (E) Liver sections stained with H&E, Sirius Red, αSMA, Krt7, OGT, SOX9, and TUNEL. Scale bars = 100 μm. (F) Relative expression levels of fibrosis markers normalised to TBP. (G) Serum levels of ALT, AST, and LDH. (H) Relative expression levels of proliferation markers normalised to TBP. (I) Relative expression levels of inflammatory markers normalised to TBP. (J) Serum levels of Cxcl1. Data are shown as mean ± SEM of 5–10 individual male mice. $^{*}p$ <0.05, $^{**}p$ <0.01, $^{***}p$ <0.001 by unpaired Student's *t* test (Mann–Whitney *U* test). αSMA, alpha-smooth muscle actin; ALT, alanine aminotransferase; AST, aspartate aminotransferase; BAT, brown adipose tissue; Ccl5, C–C motif chemokine ligand 5; Col3a1, collagen type III alpha 1 chain; Col6a1, collagen type VI alpha 1 chain; Cxcl1, C–X–C motif chemokine ligand 1; CycA2, cyclin A2; CycB1, cyclin B1; CycD1, cyclin D1; Krt7, cytokeratin 7; LDH, lactate dehydrogenase; Mcp1, monocyte chemoattractant protein-1; OGA, *O*-GlcNAcase; OGT, *O*-GlcNAc transferase; SOX9, sex determining region Y-box 2; TBP, TATA-box binding protein; TGFβ, transforming growth factor beta; Tnfα, tumour necrosis factor alpha; TUNEL, terminal deoxynucleotidyl transferase dUTP nick end labelling; WAT, white adipose tissue.

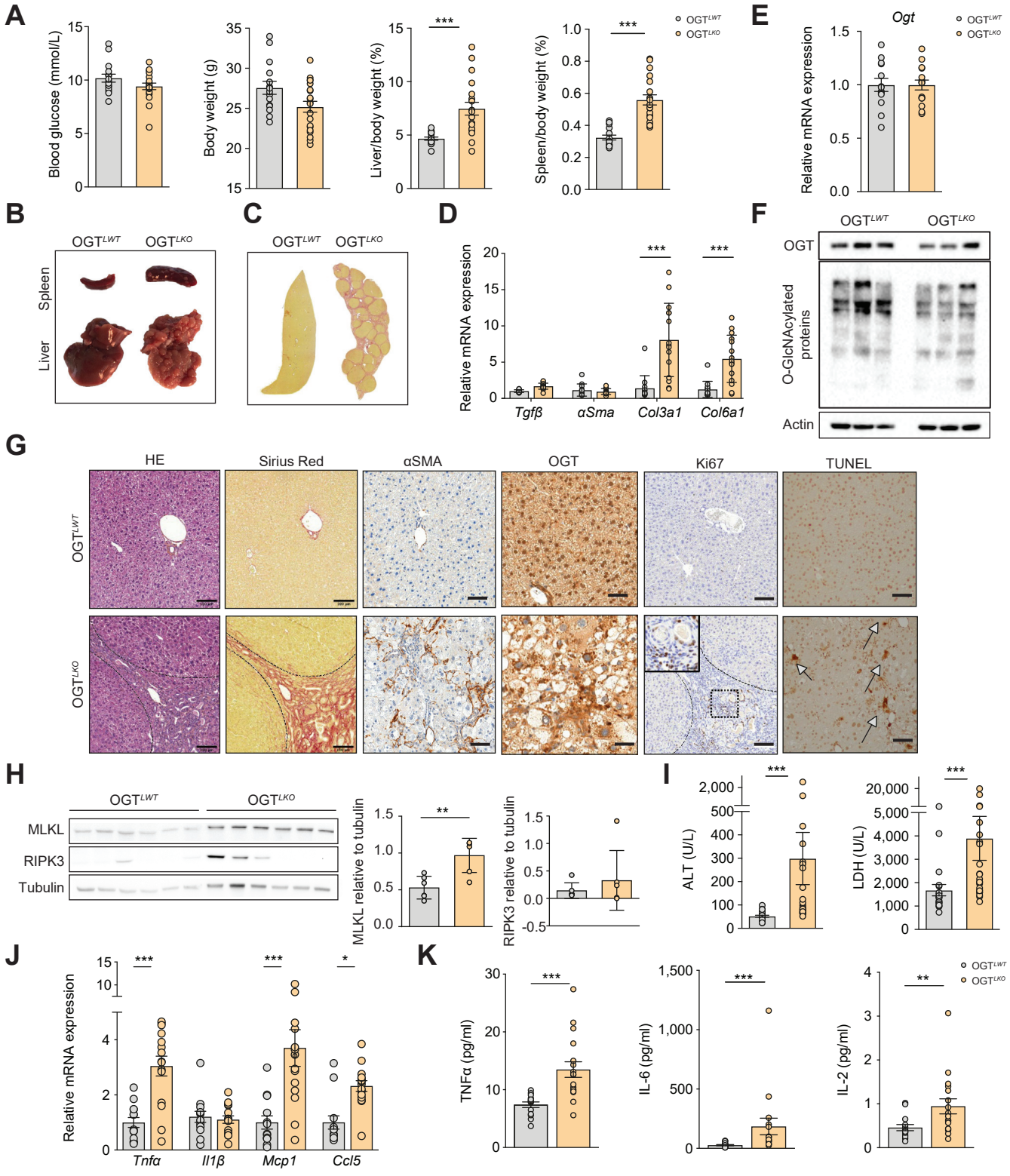

Fig. 2. OGT^{LKO} mice exhibit liver extensive fibrosis at 8 weeks. Male liver-specific *Ogt* knockout mice (OGT^{LKO}) and control floxed littermates (OGT^{LWT}) were studied 8 weeks after birth in the fed state. (A) Fed blood glucose (mmol/L), body weight (g), liver weight, and spleen weight are shown. Liver and spleen weights are represented as percentage of body weight. (B) Macroscopic view of spleen and liver from OGT^{LWT} (left) and OGT^{LKO} (right) mice. (C) Macroscopic view of histological liver section stained with Sirius Red. (D) Relative expression levels of fibrosis markers normalised to TBP. (E) Expression levels of OGT normalised to TBP. (F) Western blots of OGT content and *O*-GlcNAcylation levels in livers of OGT^{LWT} and OGT^{LKO} mice at 8 weeks. Three representative samples are shown. Actin was used for normalisation. (G) Liver sections stained with H&E, Sirius Red, αSMA, OGT, Ki67, and TUNEL. Scale bars = 100 μm. (H) Western blot analysis of necroptosis proteins (MLKL and RIPK3). Six representative samples are shown. Tubulin was used for normalisation and quantification. (I) Serum levels of ALT and LDH. (J) Relative expression levels of inflammatory markers normalised to TBP. (K) Serum levels of inflammatory cytokines. Data are shown as mean ± SEM of

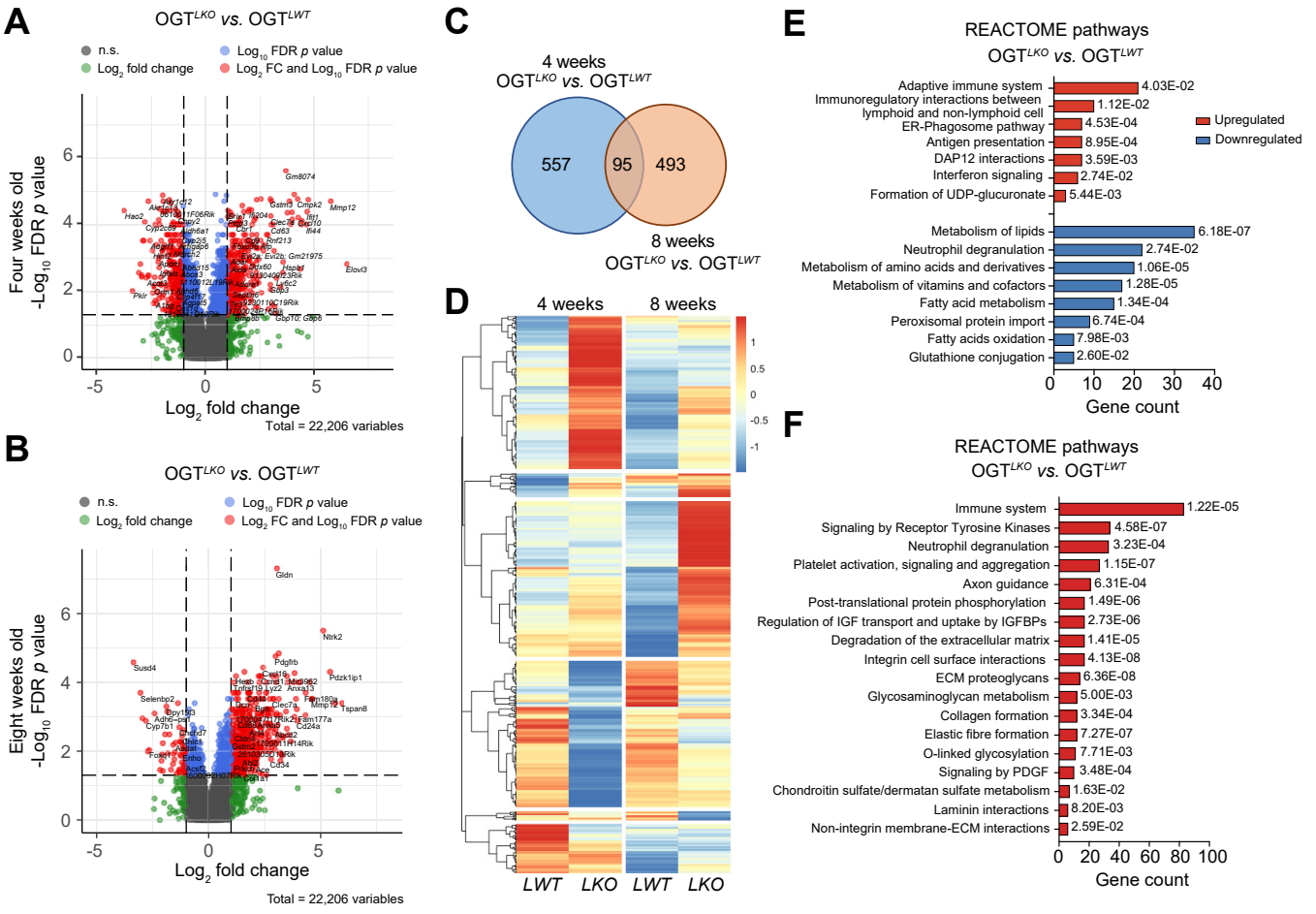

Fig. 3. Microarray analysis in liver reveals specific transcriptional changes at 4 and 8 weeks in OGT^{LKO} mice. Results were generated using microarray data from five replicates per condition. (A and B) Volcano plot representing differential gene expression of 22,206 genes comparing livers from OGT^{LKO} and OGT^{LWT} mice 4 (A) and 8 (B) weeks after birth. Log_2FC is represented in the X-axis and $log_{10}FDR$ *p* value in the Y-axis. FC ≥|2| and FDR *p* value <0.05 were taken as cut-off parameters for selection of DE genes, represented in red. (C) Venn diagram of DE genes in the liver of 4- and 8-week-old mice. (D) Hierarchical clustering showing differential expression of genes in liver of OGT^{LKO} mice compared with OGT^{LWT} mice. (E and F) Top Reactome pathways significantly upregulated or downregulated using the DE genes between male OGT^{LKO} and OGT^{LWT} mice at 4 (E) or 8 (F) weeks. DE, differentially expressed; ECM, extracellular matrix; ER, endoplasmic reticulum; FC, fold change; FDR, false discovery rate; IGFBP, insulin-like growth factor binding protein; OGT, *O*-GlcNAc transferase; PDGF, platelet-derived growth factor.

between the two groups of mice (Fig. 1G). The expression of proliferation markers was also significantly induced in the liver of OGT^{LKO} mice compared with OGT^{LWT} mice (*Ki67*, *CycA2*, cyclin B1 [*CycB1*], and *CycD1*) (Fig. 1H). To investigate the potential development of inflammation in the context of liver injury, we examined the expression of inflammatory markers. Significant induction of tumour necrosis factor alpha (*Tnfa*), monocyte chemoattractant protein-1 (*Mcp1*), and C–C motif chemokine ligand 5 (*Ccl5*) was observed in the liver of OGT^{LKO} compared with OGT^{LWT} mice (Fig. 1I). Analyses of serum pro-inflammatory cytokine and chemokine levels in 4-week-old mice also revealed a significant increase in C–X–C motif chemokine ligand 1 (Cxcl1) concentration (Fig. 1J). Altogether, these results reveal that constitutive hepatic deletion of OGT in mice rapidly triggers early signs of liver injury, as illustrated by the onset of inflammation, apoptosis, and moderate fibrosis at 4 weeks of age.

OGT^{LKO} mice exhibit necroptosis, extensive liver fibrosis, and liver injury at 8 weeks

To determine whether the emerging phenotype of liver injury observed in 4-week-old OGT^{LKO} mice worsens with time, both male (Fig. 2 and Fig. S2) and female (Fig. S3) OGT^{LKO} mice were studied 8 weeks after birth. Similar blood glucose concentrations and body weights were observed in 8-week-old male OGT^{LWT} and OGT^{LKO} mice (Fig. 2A), whereas both liver and spleen weights were significantly increased in OGT^{LKO} mice compared with OGT^{LWT} mice, regardless of sex (Fig. 2A). Interestingly, a dysmorphic liver with hepatic nodules together with

13–15 male mice per condition. **p* <0.05, ***p* <0.01, ****p* <0.001 by unpaired Student's *t* test (Mann–Whitney *U* test). αSMA, alpha-smooth muscle actin; ALT, alanine aminotransferase; Ccl5, C–C motif chemokine ligand 5; Col3a1, collagen type III alpha 1 chain; Col6a1, collagen type VI alpha 1 chain; LDH, lactate dehydrogenase; Mcp1, monocyte chemoattractant protein-1; MLKL, mixed lineage kinase domain-like pseudokinase; OGT, *O*-GlcNAc transferase; RIPK3, receptor-interacting serine/threonine-protein kinase 3; TBP, TATA-box binding protein; Tgfβ, transforming growth factor beta; Tnfα, tumour necrosis factor alpha; TUNEL, terminal deoxynucleotidyl transferase dUTP nick end labelling.

splenomegaly was observed macroscopically at sacrifice in a large proportion of OGT^{LKO} mice (Fig. 2B). The macroscopic view of the histological liver section of OGT^{LKO} mice from Sirius Red staining showed a homogeneous distribution of these nodules, which were identified as regeneration nodules typical of chronically injured livers (Fig. 2B and C). Of note, clear signs of advanced hepatic fibrosis were observed in OGT^{LKO} liver sections, regardless of the presence of macroscopic regenerative nodules (Fig. S2D). In agreement, mRNA levels of fibrosis markers (*Col3a1* and *Col6a1*) were significantly increased in both male and female

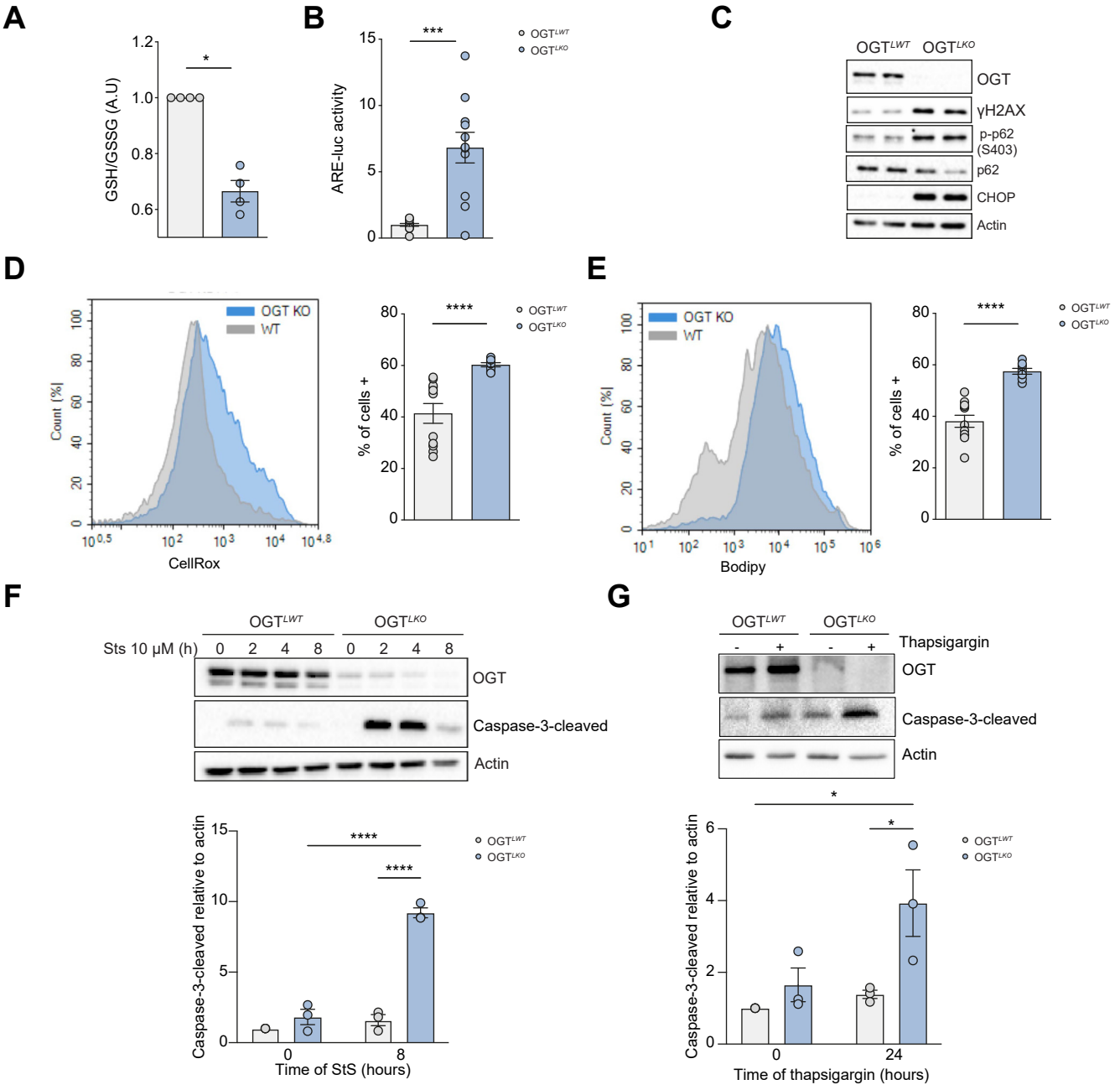

Fig. 4. Hepatic OGT deficiency leads to oxidative stress, ER stress, DNA damage, and enhanced sensitivity to cell death. Experiments were performed in primary cultured hepatocytes from 4-week-old male and female mice. (A) Ratio of GSH/GSSG. (B) NRF2 activity measured upon transfection with a plasmid containing a 3 × ARE luciferase NRF2 reporter gene. (C) Western blot analysis of OGT, markers of oxidative stress, ER stress, and DNA damage markers. Two representative samples are shown. (D) Total ROS levels measured by CellRox (Ozyme). (E) Lipid peroxidation analysed by flow cytometry-based BODIPY 581/591 assays (Molecular Probes). (F) Western blot analysis of OGT and cleaved caspase-3 after 8 h of StS treatment. Actin was used as a loading control, and quantification for 8 h post StS treatment is shown. (G) Western blot analysis of OGT and cleaved caspase-3 after 24 h of thapsigargin treatment. Actin was used as a loading control, and quantification for cleaved caspase-3 is shown. Data are shown as mean ± SEM of two to five independent cultures done in triplicate. $^{*}p$ <0.05, $^{***}p$ <0.001, $^{****}p$ <0.0005 by unpaired Student's *t* test (Mann–Whitney *U* test) (panels A, B, D, E). $^{*}p$ <0.05, $^{****}p$ <0.0005 by two-way Anova followed by Bonferroni *post hoc* test (panels F and G). ARE, antioxidant response element; CHOP, CCAAT–enhancer-binding protein homologous protein; ER, endoplasmic reticulum; GSH, reduced glutathione; GSSG, oxidised glutathione; H2AX, H2AX variant histone; NRF2, nuclear factor erythroid-derived 2-related factor; OGT, *O*-GlcNAc transferase; ROS, reactive oxygen species; StS, staurosporine.

OGT^{LKO} mice (Fig. 2D and Fig. S3F), and parallel Sirius Red and αSMA staining showed fibroblast activation and advanced fibrosis in OGT^{LKO} livers (Fig. 2G and Fig. S3D). Surprisingly, analysis of OGT mRNA and protein levels revealed recovery of OGT expression in livers of OGT^{LKO} mice compared with OGT^{LWT} mice, despite a less pronounced effect in females than in males (Fig. 2E and F and Fig. S3C). However, OGT immunolabelling showed OGT-positive cells in OGT^{LKO} liver sections regardless of sex (Fig. 2G and Fig. S3D), suggesting counterselection against OGT-deficient cells during liver regeneration.[19] The emergence of

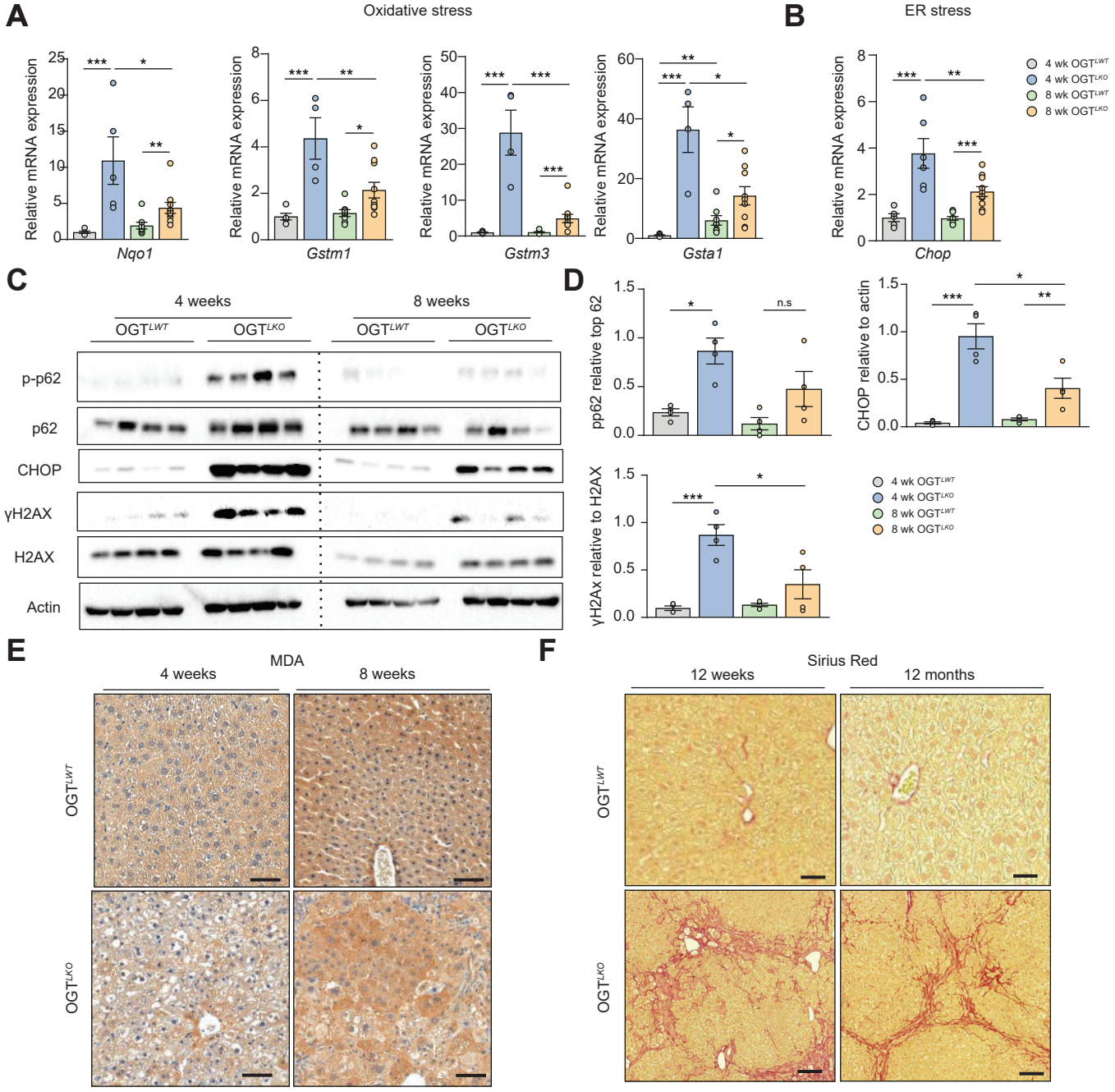

Fig. 5. Oxidative stress, ER stress, lipid peroxidation, and DNA damage in livers of 4 and 8 weeks old OGT^{LKO} mice. Male liver-specific *Ogt* knockout mice (OGT^{LKO}) and control floxed littermates (OGT^{LWT}) were studied 4 and 8 weeks after birth in the fed state. (A) Relative expression levels of oxidative stress markers normalised to TBP. (B) Relative expression of *Chop* normalised to TBP. (C) Western blots showing protein content in whole liver lysates of markers of oxidative stress (p-p62), ER stress (CHOP), and DNA damage (γH2AX) normalised to actin. Cropped membranes are indicated with discontinued lines. (D) Quantification of p-p62, CHOP, and γH2AX is shown. (E) MDA staining in liver sections from 4- and 8-week-old OGT^{LWT} and OGT^{LKO} mice. Scale bars = 100 μm. (F) Liver sections from OGT^{LWT} and OGT^{LKO} mice at 12 weeks and 12 months of age stained with Sirius Red. Scale bars = 100 μm. Data are shown as mean ± SEM of 8–10 mice at 4 weeks, 13–15 mice at 8 weeks, 18–20 mice at 12 weeks, and 18–20 mice at 1 year. $^{*}p$ <0.05, $^{**}p$ <0.01, $^{***}p$ <0.001 by two-way Anova followed by Bonferroni *post hoc* test. CHOP, CCAAT–enhancer-binding protein homologous protein; ER, endoplasmic reticulum; Gsta1, glutathione S-transferase alpha 1; Gstm1, glutathione S-transferase mu 1; Gstm3, glutathione S-transferase mu 3; H2AX, H2AX variant histone; MDA, malondialdehyde; NqO1, NAD(P)H quinone dehydrogenase 1; OGT, *O*-GlcNAc transferase; TBP, TATA-box binding protein.

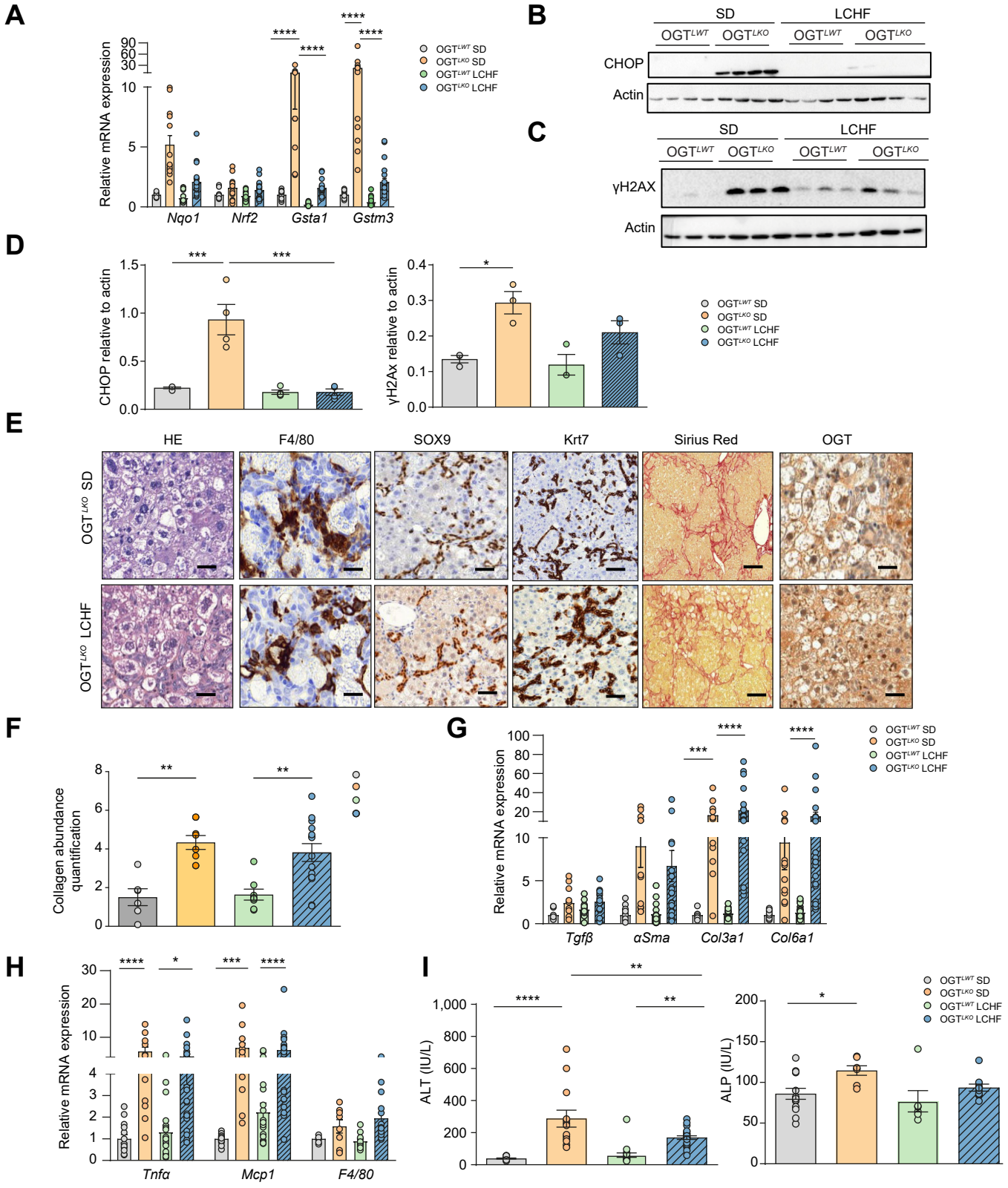

Fig. 6. LCHF diet improves oxidative stress, ER stress, and DNA damage but not fibrosis in OGT^{LKO} mice. Liver-specific *Ogt* knockout mice (OGT^{LKO}) and control floxed littermates (OGT^{LWT}) (males and females) were weaned (at 3 weeks of age) on an LCHF diet and sacrificed 5 weeks later in the fed state. (A) Relative expression levels of oxidative stress markers normalised to TBP. (B) Western blot analysis of CHOP protein content in livers of OGT^{LWT} and OGT^{LKO} mice on either SD or LCHF diet. Four representative samples are shown. (C) Western blot analysis of γH2AX protein content in livers of OGT^{LWT} and OGT^{LKO} mice on either SD or LCHF diet. Three representative samples are shown. (D) Quantification of CHOP and γH2AX is shown. Actin was used as a loading control. (E) Liver sections stained with H&E, F4/80, SOX9, Krt7, Sirius Red, and OGT. Scale bars = 100 μm. (F) Quantification of fibrosis SHG microscopy. (G) Relative expression levels of fibrosis

TUNEL-positive cells in OGT^{LKO} liver sections as well as Ki67-positive cells in hepatic tissue surrounding the regenerative nodules of OGT^{LKO} livers (Fig. 2G) suggested an activation of both proliferation and apoptosis pathways. Accordingly, the expression of proliferation markers was significantly induced in livers of OGT^{LKO} mice compared with OGT^{LWT} mice at both mRNA (*Ki67*, *CycA2*, *CycB1*, and *CycD1*) and protein levels (cyclin A, cyclin D1, and PCNA) (Fig. S2C and Fig. 2C). Although the expression of RIPK3 was unchanged in OGT^{LKO} livers, the expression of MLKL, another key protein of necroptosis, was significantly increased (Fig. 2H). In agreement, OGT^{LKO} mice exhibited a significant increase in plasma ALT and LDH concentrations (Fig. 2I), whereas the circulating levels of AST, another marker of liver injury, was unchanged (Fig. S3E). The expression of inflammatory markers (*Tnfα*, *Mcp1*, and *Ccl5*) and plasma concentrations of cytokines (TNFα, IL-2, and IL-6) were also increased in livers of OGT^{LKO} mice compared with the OGT^{LWT} control group (Fig. 2J and K). A similar phenotype comprising inflammation, fibrosis, and liver injury was observed in 8-week-old OGT^{LKO} female mice (Fig. S3H and Fig. 3H). Therefore, either males or females, or both, were used in further experiments, as indicated in the figure legends. Finally, we next investigated whether OGT^{LKO} liver alterations were associated with early (4 weeks) or later (8 weeks) changes in cell identity following deletion of hepatic OGT (Fig. S2F). A marked increase in mRNA levels of progenitor cells and cholangiocyte markers, *Krt7* and *Krt19*, was observed in livers of OGT^{LKO} mice compared with OGT^{LWT} mice of both ages, although differences were more pronounced at 8 weeks (Fig. S2G). Immunolabelling of HNF4α, SOX9, and Krt19 on liver sections confirmed a ductular reaction, mostly localised in the fibrosis septa in older OGT^{LKO} mice (Fig. S2H). Whereas total or direct bilirubin was not changed, a significant increase in serum ALP was measured in 8-week-old OGT^{LKO} mice compared with OGT^{LWT} mice (Fig. S2E). Taken together, our results suggest that OGT plays an important role in liver cell identity and that its deficiency leads to a rapid deterioration of liver homeostasis in OGT^{LKO} mice.

Hepatocyte OGT deletion leads to specific transcriptional changes in the liver from 4- and 8-week-old OGT^{LKO} mice

To better characterise the early and late consequences of hepatic OGT deficiency, we performed a transcriptomic analysis on livers from 4- and 8-week-old OGT^{LKO} and OGT^{LWT} mice. Volcano plots, which were generated by using a total of 22,206 hepatic genes and by comparing OGT^{LKO} mice with OGT^{LWT} mice, demonstrated a shift in the expression levels of specific genes between the two time points studied (4 and 8 weeks) (Fig. 3A and B). The Venn diagram (fold change ≥|2|, FDR *p* value <0.05) indicated that 557 and 493 genes were differentially expressed at 4 and 8 weeks, respectively, with 95 differentially expressed genes common to 4- and 8 -week-old mice (Fig. 3C and Table S3). Several gene clusters were differentially regulated in OGT^{LKO} livers as compared with OGT^{LWT} livers at 4 and 8 weeks, as illustrated by the heatmap analysis (Fig. 3D). Analysis of Reactome pathways in the liver of 4-week-old mice showed a significant downregulation in basic metabolic pathways such as lipid, amino acid, and vitamin metabolism (Fig. 3E). Interestingly, the glutathione metabolism pathway, an important detoxification pathway in the liver,[20] was also significantly downregulated at this stage (Fig. 3E). In parallel, the expression of genes involved in immune signalling pathways and UDP-glucuronate formation, the latest known to be activated during antioxidant response in the liver,[21] were upregulated at 4 weeks in OGT^{LKO} mice (Fig. 3E). Surprisingly, analysis of differentially expressed genes at 8 weeks only reported upregulated pathways. Upregulation of genes involved in immune system activation suggested that the inflammation response was not resolved at 8 weeks. However, an upregulation of pathways involved in liver injury and its resolution such as formation and degradation of extracellular matrix was observed (Fig. 3F and Fig. S4D). Altogether, the results indicate specific changes in global mRNA expression occurring between 4 and 8 weeks, indicating early and major molecular adaptations in the liver to cope with the loss of hepatic OGT.

OGT deficiency in hepatocytes leads to oxidative stress, ER stress, and enhanced sensitivity to cell death

Given that the transcriptomic analysis revealed that a cluster of DE genes involved in the oxidative stress response was significantly upregulated in OGT^{LKO} livers at 4 weeks (Fig. S4A), we performed experiments in primary hepatocytes isolated from 4-week-old OGT^{LKO} mice. Interestingly, the GSH/GSSG ratio, a reliable indicator of oxidative stress, was significantly decreased in OGT^{LKO} hepatocytes compared with OGT^{LWT} hepatocytes, supporting enhanced hepatic oxidative stress response in 4-week-old OGT^{LKO} mice (Fig. 4A). Because oxidative stress response involves binding of nuclear factor erythroid-derived 2-related factor 2 (NRF2) on ARE located on promoters of antioxidant response genes, we monitored NRF2 activity in OGT^{LKO} and OGT^{LWT} hepatocytes, by using an ARE luciferase reporter construct.[16] ARE luciferase activity was increased by sevenfold in OGT^{LKO} hepatocytes compared with OGT^{LWT} hepatocytes, suggesting that the NRF2 antioxidant response was induced in the absence of OGT (Fig. 4B). In agreement, an increase in p-p62 (autophagy-related oxidative stress),[22,23] γH2AX (DNA damage), and CHOP (ER stress-derived apoptosis) was observed in hepatocytes from OGT-deficient cells compared with OGT^{LWT} hepatocytes (Fig. 4C). To further characterise oxidative stress in OGT^{LKO} hepatocytes, total ROS and total lipid peroxidation were assayed using CellROX and BODIPY assays. Both parameters were found significantly increased in OGT^{LKO} hepatocytes compared with OGT^{LWT} hepatocytes (Fig. 4D and E). Sensitivity of OGT^{LKO} hepatocytes to oxidative stress-dependent apoptosis was next evaluated over an 8-h time course in primary hepatocytes treated with StS[24] (Fig. 4F). Higher levels of cleaved caspase-3, a marker of apoptosis, were observed in OGT-deficient cells compared with OGT^{LWT} hepatocytes upon StS treatment, indicating enhanced sensitivity to StS-induced cell

markers normalised to TBP. (H) Relative expression levels of inflammatory markers normalised to TBP. (I) Serum levels of ALT and ALP. Data are shown as mean ± SEM of 4–13 mice (males and females). $^{*}p$ <0.05, $^{**}p$ <0.01, $^{***}p$ <0.001, $^{****}p$ <0.0005 by two-way Anova followed by Bonferroni *post hoc* test. αSMA, alpha-smooth muscle actin; ALP, alkaline phosphatase; ALT, alanine aminotransferase; CHOP, CCAAT–enhancer-binding protein homologous protein; Col3a1, collagen type III alpha 1 chain; Col6a1, collagen type VI alpha 1 chain; ER, endoplasmic reticulum; Gsta1, glutathione S-transferase alpha 1; Gstm3, glutathione S-transferase mu 3; H2AX, H2AX variant histone; Krt7, cytokeratin 7; LCHF, low-carbohydrate, high-fat; Mcp1, monocyte chemoattractant protein-1; NqO1, NAD(P)H quinone dehydrogenase 1; NRF2, nuclear factor erythroid-derived 2-related factor; OGT, *O*-GlcNAc transferase; SD, standard diet; SHG, second harmonic generation; SOX9, sex-determining region Y-box 2; TBP, TATA-box binding protein; TNFα, tumour necrosis factor alpha.

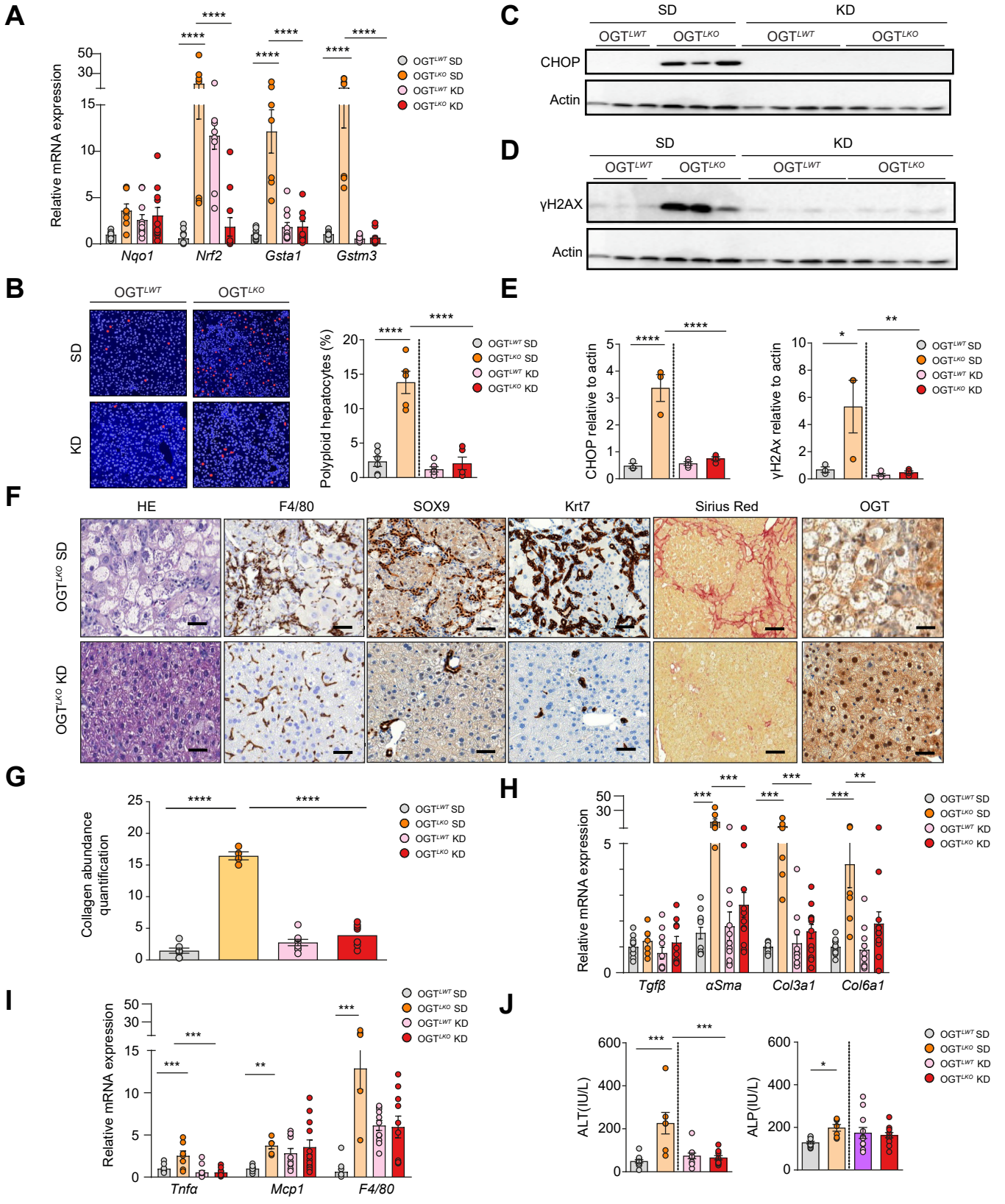

Fig. 7. KD improves oxidative stress, ER stress, DNA damage, hepatic fibrosis, and liver injury in OGT^{LKO} mice. Liver-specific *Ogt* knockout mice (OGT^{LKO}) and control floxed littermates (OGT^{LWT}) (males and females) were weaned (at 3 weeks of age) on KD and sacrificed 5 weeks later in the fed state. (A) Relative expression levels of oxidative stress markers normalised to TBP. (B) The proportion of highly polyploid (≥8n) mononuclear hepatocytes relative to total hepatocytes was quantified in each group. Blue: plasma membrane labelling (KL1). Red: nuclear labelling (Hoechst) (scale bar = 100 μm). (C) Western blot analysis of CHOP protein content in livers of OGT^{LWT} and OGT^{LKO} mice. Three to four representative samples are shown. (D) Western blot analysis of γH2AX protein content in livers of OGT^{LWT}

death (Fig. 4F). Similarly, sensitivity to ER stress-induced apoptosis was also enhanced in OGT^{LKO} hepatocytes compared with OGT^{LWT} hepatocytes, as illustrated by significantly higher levels of cleaved caspase-3 observed upon thapsigargin treatment (24 h) (Fig. 4G). Altogether, these data demonstrate that OGT deficiency promotes early oxidative and ER stress, leading to DNA damage and increased hepatocyte sensitivity to cell death.

OGT^{LKO} mice display extensive and prolonged hepatic fibrosis in response to early oxidative and ER stress

Aiming at better characterising the phenotype of oxidative and ER stress in the OGT^{LKO} mice *in vivo*, we measured oxidative stress markers by qPCR in livers of 4- and 8-week-old OGT^{LKO} mice (Fig. 5). These results confirmed a set of genes significantly induced at not only 4 weeks (NAD[P]H quinone dehydrogenase 1 [*Nqo1*], glutathione S-transferase mu 1 [*Gstm1*], glutathione S-transferase mu 3 [*Gstm3*], and glutathione S-transferase alpha 1 [*Gsta1*]) but also 8 weeks in livers of OGT^{LKO} mice, although to a lesser extent at 8 weeks than at 4 weeks (Fig. 5A and B). Similar changes were observed at the protein level for mediators of the oxidative/ER stress response (p-62 and CHOP) and DNA damage (γH2AX) (Fig. 5C and D). To better characterise the phenotype observed in OGT^{LKO} mice, we performed kinetic experiments and included an earlier time point (2 weeks) (Fig. S5). The inflammation state occurred as early as 2 weeks after birth, with evidence of increased phosphorylation of JNK in livers of 2-week-old OGT^{LKO} mice (Fig. S5A). Of note, mRNA levels of oxidative stress (*Nqo1*, *Gstm1*, and *Gstm3*) and ER stress markers (*Chop*) were significantly increased later on, between 4 and 8 weeks after birth (Fig. S5A and B). However, staining with MDA, a commonly used marker for lipid peroxidation,[25] revealed positive staining on liver sections from 8-week-old OGT^{LKO} compared with OGT^{LWT} mice, confirming sustained hepatic stress at this stage of development (Fig. 5E). Finally, to better characterise the long-term progression of hepatic damages in OGT^{LKO} mice, we followed mice up to 12 months and sacrificed them at specific time points (8 weeks, 12 weeks, and 12 months). Although the expression of oxidative stress and inflammation markers was found increased in livers of OGT^{LKO} mice compared with OGT^{LWT} mice at 12 weeks, no difference between the two genotypes was observed when the mice were analysed at 12 months (Fig. S6B and Fig. 6D). In contrast, Sirius Red staining revealed marked residual hepatic fibrosis in both 12-week-old and 12-month-old OGT^{LKO} mice (Fig. 5F). In agreement, ALT serum levels were significantly increased in 12-week-old and 12-month-old OGT^{LKO} mice compared with controls (Fig. S6E). Taken together, these data suggest that inflammation and oxidative stress are early triggering events of the OGT^{LKO} phenotype peaking between 2 and 4 weeks, respectively. However, the rest of hepatic alterations of OGT^{LKO} mice (namely, fibrosis and liver injury) persisted over time.

LCHF diet prevents hepatic oxidative stress, ER stress, and DNA damage in OGT^{LKO} mice

During the suckling period, pups receive an LCHF diet that switches to a SD containing nearly 70% of carbohydrates at weaning. Because no oxidative stress was observed in livers of 2-week-old OGT^{LKO} mice, that is, during the suckling period, we hypothesised that the elevated oxidative stress observed at 4 weeks could result from elevated carbohydrate content in the diet at weaning. Therefore, OGT^{LWT} and OGT^{LKO} mice were weaned and maintained for 5 weeks on either a SD (69% of carbohydrates, 4% of fat, and 26% of proteins) or an LCHF diet compensated by lipid enhancement (21% of carbohydrates, 60% of fat, and 19% of proteins) (Fig. 6 and Fig. S7A). Induction of oxidative stress markers (*Gsta1* and *Gstm3*) in livers of OGT^{LKO} mice compared with OGT^{LWT} mice on SD (OGT^{LKO} SD *vs.* OGT^{LWT} SD) was significantly reduced when OGT^{LKO} mice were fed with LCHF diet (OGT^{LKO} LCHF) (Fig. 6A). Interestingly, the expression of ER stress (CHOP) and DNA damage markers (γH2AX) was also reduced in livers of OGT^{LKO} LCHF mice when compared with OGT^{LKO} SD (Fig. 6B–D and Fig. S7D). OGT immunostaining revealed significant staining in liver sections from OGT^{LKO} mice regardless of the nutritional conditions (Fig. 6E) in agreement with the re-expression observed on SD diet (Fig. 2E and F). Histological analysis of liver ballooning (H&E), inflammation (F4/80), ductular reaction (SOX9, Krt7), and fibrosis (Sirius Red) showed no evidence of improvement upon LCHF conditions (Fig. 6E). Quantification of fibrosis revealed similar hepatic fibrosis in OGT^{LKO} mice compared with OGT^{LWT} mice under either SD or LCHF diet (Fig. 6F). In agreement, the expression of inflammatory markers (*Tnfa* and *Mcp1*) and fibrosis markers (*Col3a1* and *Col6a1*) was found similarly increased in livers of OGT^{LKO} mice compared with OGT^{LWT} mice in both nutritional challenges (Fig. 6H and G). Nevertheless, a significant reduction in liver injury marker ALT was observed when OGT^{LKO} mice were weaned on an LCHF diet (Fig. 6I), and a tendency towards reduced circulating levels of inflammatory cytokine Cxcl1 was also noted (Fig. S7E). As specific lipids could contribute to oxidative stress and/or ER stress, the hepatic lipidomic profiling (including triglycerides, cholesterol, sphingolipids, and fatty acids) of LCHF diet-fed mice *vs.* SD-fed mice was performed (Fig. S9A). Lipidomic analysis revealed that the majority of lipid species changes was caused by the dietary change rather than by the genotype (clusters 1, 2, 4, and 5; Fig. S9A). However, clusters 3 and 7 highlighted lipid signatures that were respectively more and less abundant in OGT^{LKO} mice fed an LCHF diet compared with SD.

Taken together, these results suggest that although weaning OGT^{LKO} mice on an LCHF diet improved some parameters of liver damages (oxidative stress, ER stress, and DNA damage), it failed to fully prevent hepatic alterations, such as ballooning, inflammation, ductular reaction, and fibrosis.

and OGT^{LKO} mice. Three to four representative samples are shown. (E) Quantification of CHOP and γHA2X are shown. Actin was used as a loading control. (F) Liver sections stained with H&E, F4/80, SOX9, Krt7, Sirius Red, and OGT. Scale bars = 100 μm. (G) Quantification of fibrosis by SHG microscopy. (H) Relative expression levels of fibrotic markers normalised to TBP. (I) Relative expression levels of inflammatory markers normalised to TBP. (J) Serum levels of ALT and ALP. Data are shown as mean ± SEM of four to eight mice (males and females). *p <0.05, **p <0.01, ***p <0.001, ****p <0.0005 by two-way Anova followed by Bonferroni *post hoc* test. αSMA, alpha-smooth muscle actin; ALP, alkaline phosphatase; ALT, alanine aminotransferase; CHOP, CCAAT–enhancer-binding protein homologous protein; Col3a1, collagen type III alpha 1 chain; Col6a1, collagen type VI alpha 1 chain; ER, endoplasmic reticulum; Gsta1, glutathione S-transferase alpha 1; Gstm3, glutathione S-transferase mu 3; H2AX, H2AX variant histone; KD, ketogenic diet; Krt7, cytokeratin 7; Mcp1, monocyte chemoattractant protein-1; NqO1, NAD(P)H quinone dehydrogenase 1; Nrf2, nuclear factor erythroid-derived 2-related factor; OGT, *O*-GlcNAc transferase; SD, standard diet; SHG, second harmonic generation; SOX9, sex-determining region Y-box 2; TBP, TATA-box binding protein; Tgfβ, transforming growth factor beta; Tnfα, tumour necrosis factor alpha.

KD prevents the hepatic alterations of OGT^{LKO} mice

Given that the LCHF diet still contains 21% of carbohydrates, we hypothesised that further decreasing the carbohydrate content in the diet could improve the severe liver damage in OGT^{LKO} mice. Therefore, OGT^{LWT} and OGT^{LKO} mice were challenged at weaning with a KD for 5 weeks (1% of carbohydrates, 94% of fat, and 5% of protein) (Fig. S8A). Significant induction of oxidative stress markers (*Gsta1* and *Gstm3*) in livers of OGT^{LKO} mice compared with OGT^{LWT} controls on SD (OGT^{LKO} SD *vs.* OGT^{LWT} SD) was significantly reduced when OGT^{LKO} mice were weaned on a KD (Fig. 7A). Because oxidative stress has been shown to promote hyperpolyploidisation of hepatocytes,[11] we quantified highly polyploid (≥8n) mononuclear hepatocytes relative to total hepatocytes in each group of mice. Although the number of highly polyploid hepatocytes was significantly increased in livers of OGT^{LKO} SD mice when compared with OGT^{LWT} SD control (Fig. 7B), no difference was observed between OGT^{LKO} and OGT^{LWT} mice when fed on KD (Fig. 7B), demonstrating that KD prevents the oxidative stress response upon hepatic OGT deficiency. The expression of ER stress (CHOP) and DNA damage (γH2AX) markers was also significantly reduced in the liver of OGT^{LKO} KD mice when compared with OGT^{LKO} SD mice (Fig. 7C–E and Fig. S8D). OGT immunostaining revealed significant staining in liver sections from OGT^{LKO} mice regardless of the nutritional conditions (Fig. 7F). Of note, in contrast to the histological observations made on an LCHF diet, liver ballooning (H&E), inflammation (F4/80), ductular reaction (SOX9 and Krt7), and fibrosis (Sirius Red) were markedly improved in OGT^{LKO} mice upon KD conditions (Fig. 7F). Quantification of fibrosis accordingly revealed a statistical decrease in hepatic fibrosis in OGT^{LKO} KD mice compared with OGT^{LKO} SD mice (Fig. 7G). In agreement, the expression of fibrosis markers (*αSma*, *Col3a1*, and *Col6a1*) was found similarly decreased in livers of OGT^{LKO} KD mice compared with OGT^{LKO} SD mice (Fig. 7H). F4/80 staining showed a marked reduction in liver sections from OGT^{LKO} KD mice compared with OGT^{LKO} SD mice (Fig. 7F). Lastly, a significant difference was observed for liver injury marker ALT when OGT^{LKO} mice were weaned on a KD (Fig. 7J). Interestingly, we also observed that specific hepatic lipid species previously associated with liver apoptosis and fibrosis (Cer C24:0 and C24:1)[26,27] were no longer increased when OGT^{LKO} mice were weaned on a KD (Fig. S9B). Altogether, these results show that weaning on a KD fully prevented the phenotype of the OGT^{LKO} mice (oxidative stress, polyploidy, ER stress, inflammation, fibrosis, and liver injury).

Discussion

In the liver, *O*-GlcNAcylation has emerged as an important regulatory mechanism underlying normal liver physiology and metabolic disease.[1] We previously reported that *O*-GlcNAcylation of two key transcription factors involved in glucose and lipid metabolism (*i.e.* ChREBP and Foxo1) significantly contributes to gluco-lipotoxicity in hepatocytes.[3,4] However, the function of OGT in liver sensing appears rather complex as other studies reported that OGT is rather involved in the survival and death balance in hepatocytes, and also suggested that OGT acts as a critical modulator of hepatocyte homeostasis in the context of liver injury and/or chronic liver diseases.[5,28]

To better understand the importance of *O*-GlcNAcylation signalling in hepatocytes, we generated mice with a liver-specific constitutive deletion of OGT (OGT^{LKO} mice) and examined their phenotype over a time course ranging from 2 weeks to 1 year upon different dietary challenges. Our specific goal was to address whether the lack of OGT could lead to oxidative stress and associated liver injuries in a diet-dependent manner. We first evaluated glucose homeostasis parameters and observed a significant decrease in fasting blood glucose levels, as well as an improvement in both glucose and pyruvate tolerances when comparing OGT^{LKO} with OGT^{LWT} mice at 4 weeks of age. In agreement, the expression of gluconeogenic genes was significantly decreased in OGT^{LKO} livers. Interestingly, the *O*-GlcNAcylation of Foxo1, a modification previously shown to regulate its transcriptional activity towards its target gluconeogenic genes,[4,29] was significantly decreased in livers of 4-week-old OGT^{LKO} mice compared with OGT^{LWT} mice. However, despite improvement in metabolic homeostasis, clear signs of liver injury were already detectable at 4 weeks with a significant increase in proliferation markers, elevated inflammation, and moderate fibrosis, suggesting a critical role for OGT in preventing hepatocyte insult. Indeed, experiments in cultured OGT^{LKO} hepatocytes also confirmed oxidative stress, the later evidenced by a significant decrease in the GSH/GSSG ratio, elevated total ROS production, and lipid peroxidation. Follow-up analysis of OGT^{LKO} mice demonstrated the development of hepatomegaly, advanced fibrosis, and cholestasis, features that persisted in 1-year-old OGT^{LKO} mice and that are usually seen in bile duct ligation models.[30] Importantly, this severe hepatic phenotype was observed in both male and female OGT^{LKO} mice, underlining the importance of using both sexes in experimental research to better understand how and why some diseases and conditions affect men and women differently. Interestingly, although recent studies have revealed the existence of sexual dimorphisms in liver diseases, in particular in non-alcoholic fatty liver disease and fibrosis onset,[31,32] we could not see any significant evidence when comparing the phenotype of OGT^{LKO} males with that of OGT^{LKO} females.

The phenotype of liver OGT deficiency in hepatocytes also led to changes in cell identity profile, probably favouring the differentiation of hepatoblasts to cholangiocytes, typical of the ductular reaction produced in the initial steps of liver regeneration.[33] Interestingly, a higher number of highly polyploid hepatocytes was observed in livers of 8-week-old OGT^{LKO} mice. Although polyploidisation can represent a gain of function by contributing to tissue differentiation, we believe that the hyperpolyploidisation observed was caused by extensive cellular stress and can be considered here as a pathological lesion, as previously suggested in other mouse models of hepatic oxidative stress.[34]

A surprising observation was the partial recovery of OGT expression at 8 weeks of age in livers of OGT^{LKO} mice. A similar phenomenon, which could be linked to counterselection[19] of OGT-expressing cells, has already been described for other liver-specific gene knockout models.[35–37] Indeed, hepatocytes deficient in OGT may encounter difficulties to survive in an oxidative and inflammatory environment and enter a process of cell death, whereas hepatocytes escaping to the recombination process will repopulate the liver with cells expressing OGT protein. In agreement with this hypothesis, higher sensitivity to cell death inducers was observed in OGT^{LKO} hepatocytes compared with OGT^{LWT} hepatocytes. This increased susceptibility to cell death

upon defective *O*-GlcNAcylation is consistent with the significant necroptosis observed following liver OGT deletion[5] and with enhanced necroptosis and apoptosis in livers of OGT-deficient mice after partial hepatectomy.[28] Several other mouse models with liver-specific deficiency in proteins involved in DNA damage (such as damage-specific DNA binding protein 1 [DDB1]),[35] liver regeneration (such as yes-associated protein [YAP]),[36] or epigenetic modulation (such as enhancer of zeste homologue 1 [EZH1]/enhancer of zeste homologue 2 [EZH2])[37] exhibited a phenomenon of cell competition and recovery of expression of the targeted protein. However, the exact number of cells that escape recombination and the mechanisms involved in OGT recovery were not clearly identified in the current study, and further analysis, including single-cell RNA sequencing analysis of OGT^{LKO} hepatocytes, will be necessary to investigate these important questions. It should be also mentioned that hepatic recovery of OGT was partial only in some of the groups studied, as observed in livers of female OGT^{LKO} mice. The OGT recovery was not previously described in the published model of OGT liver knockout mice,[5] but OGT expression in OGT^{LKO} mice was documented only at the age of 4 weeks in this study.

We believe that our study describes here a valuable and timely mouse model of spontaneous fibrosis that may facilitate therapeutic target identification for prevention and treatment of chronic liver disease. Indeed, induction of hepatic fibrosis in rodents requires the use of chemicals or specific diets that, although commonly used, often lack ease of use and appropriate relevance to human liver fibrosis.[38] Although efforts towards providing a better understanding of the mechanisms associated with fibrosis progression and/or regression are being made, no approved drugs are currently available for liver fibrosis *per se*. Interestingly, recent studies have highlighted that intrinsic metabolism of parenchymal cells, immune cells, and/or hepatic stellate cells is important to sustain energetic needs of phenotypic changes in the context of fibrosis.[39] In an attempt to decrease carbohydrate intake in OGT^{LKO} mice and to reduce oxidative stress associated with lack of OGT in the liver, we first took the strategy to wean OGT^{LKO} mice on an LCHF diet in which the carbohydrate percentage is reduced by over threefold when compared with that in SD (69% of carbohydrates in SD *vs*. 21% in LCHF diet). This dietary switch, although improving several parameters including oxidative stress and ER stress, did not correct the other liver alterations such as ballooning, macrophage infiltration, ductular reaction, and fibrosis. However, when carbohydrate concentrations in the diet were further reduced and restricted to 1% in KD, full prevention of oxidative stress, hyperpolyploidy, inflammation, and more importantly fibrosis and liver injury was observed. Of course, in the context of this nutritional switch, a protective role for lipids cannot be excluded, and in fact, the combination of lowering carbohydrate intake and modulating specific lipid species could have been instrumental in the beneficial effects observed. Indeed, lipidomics analysis from LCHF diet and KD experiments revealed that OGT^{LKO} mice exhibited high abundance of specific bioactive species including Cer C24:0 and C24:1 under SD conditions, species that remain low upon KD conditions, suggesting that reduction in these Cer moieties could contribute, at least in part, to the protective effect of KD on OGT^{LKO} mice. In addition, LCHF diet and KD also differ in their capacity to produce ketone bodies, especially β-hydroxybutyrate (Figs. S7C and S8C), a signalling metabolite with protective properties against oxidative stress.[40] Although ketone body metabolism can induce oxidative stress, it was reported beneficial in the long term because it initiates an adaptive response characterised by the activation of the master regulators of the cell-protective mechanism, including NRF2.[41] This results in resolving oxidative stress, by the upregulation of antioxidative and anti-inflammatory activities, improved mitochondrial function, DNA repair, and autophagy. In agreement, studies have hypothesised that activation of ketogenesis in the liver could potentially attenuate ROS-mediated non-alcoholic steatohepatitis progression.[40]

Altogether, our study shows that hepatocyte-specific deletion of OGT leads to severe liver injury, confirming that *O*-GlcNAcylation and OGT are essential for hepatocyte homeostasis and survival. Our study also validates the OGT^{LKO} mouse model as a valuable model for the study of advanced liver fibrosis. Given that the severe fibrosis of OGT^{LKO} mice was fully prevented when mice were weaned on a very LCHF diet (*i.e.* KD), our study underlines the potential interest of nutritional intervention as an antifibrogenic strategy.

Abbreviations

αSMA, alpha-smooth muscle actin; ALP, alkaline phosphatase; ALT, alanine aminotransferase; ARE, antioxidant response element; AST, aspartate aminotransferase; Ccl5, C–C motif chemokine ligand 5; Cer, ceramide; CHOP, CCAAT–enhancer-binding protein homologous protein; Col3a1, collagen type III alpha 1 chain; Col6a1, collagen type VI alpha 1 chain; Cxcl1, C–X–C motif chemokine ligand 1; CycA2, cyclin A2; CycB1, cyclin B1; CycD1, cyclin D1; DDB1, damage-specific DNA binding protein 1; DE, differentially expressed; ER, endoplasmic reticulum; EZH1, enhancer of zeste homologue 1; EZH2, enhancer of zeste homologue 2; FAME, fatty acid methyl ester; FDR, false discovery rate; Foxo1, forkhead box protein o1; G6Pase, glucose-6-phosphate dehydrogenase; GAPDH, glyceraldehyde 3-phosphate dehydrogenase; GSH, reduced glutathione; GSSG, oxidised glutathione; Gsta1, glutathione S-transferase alpha 1; Gstm1, glutathione S-transferase mu 1; Gstm3, glutathione S-transferase mu 3; H2AX, H2A histone family member XH2A histone family member X; variant histone, HNF4α; hepatocyte nuclear factor 4 alpha, JNK; c-Jun N-terminal kinase, KD; ketogenic diet, Krt7; cytokeratin 7, Krt19; cytokeratin 19, LCHF; low-carbohydrate, high-fat; LDH, lactate dehydrogenase; Mcp1, monocyte chemoattractant protein-1; MDA, malondialdehyde; MLKL, mixed lineage kinase domain-like pseudokinase; NqO1, NAD(P)H quinone dehydrogenase 1; NRF2, nuclear factor erythroid-derived 2-related factor; OGA, *O*-GlcNAcase; OGT, *O*-GlcNAc transferase; PCNA, proliferating cell nuclear antigen; PEPCK, phosphoenolpyruvate carboxykinase; qPCR, quantitative PCR; RIPK3, receptor-interacting serine/threonine-protein kinase 3; RMA, robust multichip algorithm; ROS, reactive oxygen species; SD, standard diet; SHG, second harmonic generation; SM, sphingomyelin; SOX9, sex-determining region Y-box 2; StS, staurosporine; TBP, TATA-box binding protein; TGFβ, transforming growth factor beta; TNFα, tumour necrosis factor alpha; TUNEL, terminal deoxynucleotidyl transferase dUTP nick end labelling; WGA, wheat germ agglutinin; YAP, yes-associated protein.

Financial support

PO-P was supported by the European Union's Horizon 2020 Research and Innovation Programme under the Marie Skłodowska-Curie Grant Agreement No. 675610 (current address: Drug Transport and Tumour Metabolism Lab, MRC London Institute of Medical Sciences, London, UK), and

LP was supported by AFEF (Association Française pour l'Etude du Foie) and by INSERM (Poste d'accueil). CP acknowledges the support of grants from the National Agency for Research (ANR) (ANR-20-CE14-0038 IMAGINE, ANR-20-CE14-HEPATOMORPHIC, and ANR RHU QUID NASH).

Conflicts of interest

The authors declare no conflicts of interest.

Please refer to the accompanying ICMJE disclosure forms for further details.

Authors' contributions

Performed most the experiments: PO-P, LP. Helped perform the experiments: FB, MR, IC, MM, NP, JM, PP, MC. Performed liver sections and liver immunostaining: RO, MF. Analysed and interpreted the results from the microarray data: PO-P. Prepared the figures and wrote the manuscript: CP, TI, PO-P, LP. Provided scientific advice and critical reading of the manuscript: JG, CD, SG. Conceptualised and supervised the project: CP, TI.

Data availability statement

Data sharing subject to agreement.

Acknowledgements

The authors would like to thank Dr. Hélène Gilgenkrantz and Prof. Valérie Paradis (Centre de Recherche sur l'Inflammation [CRI], Université Paris Cité) for helpful discussions. We also would like to thank the Animal Facility from the Institut Cochin Inserm U1016 and, in particular, Mathieu Benard for taking excellent care of the mice. We also thank the Institut Cochin platforms, namely, the Genomic platform (GENOM'IC), the Cytometry and Immunobiology platform (CYBIO), the 'Imagerie du vivant platform' (PIV) (Isabelle Lagoutte Franck Lager and Gilles Renault), and the Microscopy Platform (Thomas Guilbert), for fibrosis quantification. Lipidomic profiling was done in MetaToul-Lipidomique Core Facility (I2MC, Inserm 1297, Toulouse, France) from MetaToul (Toulouse metabolomics & fluxomics facilities, www.metatoul.fr), which is part of the French National Infrastructure for Metabolomics and Fluxomics MetabohUB-ANR-11-INBS-0010.

Supplementary data

Supplementary data associated with this article can be found, in the online version, at https://doi.org/10.1016/j.jhepr.2023.100878.

References

Author names in bold designate shared co-first authorship

[1] Yang X, Qian K. Protein *O*-GlcNAcylation: emerging mechanisms and functions. Nat Rev Mol Cell Biol 2017;18:452–465.
[2] Nie H, Yi W. O-GlcNAcylation, a sweet link to the pathology of diseases. J Zhejiang Univ Sci B 2019;20:437–448.
[3] **Guinez C**, **Filhoulaud G**, Rayah-Benhamed F, Marmier S, Céline Dubuquoy C, Dentin R, et al. *O*-GlcNAcylation increases ChREBP protein content and transcriptional activity in the liver. Diabetes 2011;60:1399–1413.
[4] Kuo M, Zilberfarb V, Gangneux N, Christeff N, Issad T. *O*-glycosylation of FoxO1 increases its transcriptional activity towards the glucose 6-phosphatase gene. FEBS Lett 2008;582:829–834.
[5] Zhang B, Li MD, Yin R, Liu Y, Yang Y, Mitchell-Richards KA, et al. O-GlcNAc transferase suppresses necroptosis and liver fibrosis. JCI Insight 2019;4:e127709.
[6] Du D, Shi YH, Le GW. Oxidative stress induced by high-glucose diet in liver of C57BL/6J mice and its underlying mechanism. Mol Biol Rep 2010;37:3833–3839.
[7] Mohanty P, Hamouda W, Garg R, Aljada A, Ghanim H, Dandona P. Glucose challenge stimulates reactive oxygen species (ROS) generation by leucocytes. J Clin Endocrinol Metab 2000;85:2970–2973.
[8] de Carvalho Vidigal F, Guedes Cocate P, Gonçalves Pereira L, de Cássia Gonçalves Alfenas R. The role of hyperglycemia in the induction of oxidative stress and inflammatory process. Nutr Hosp 2012;27:1391–1398.
[9] Dickinson S, Hancock DP, Petocz P, Ceriello A, Brand-Miller J. High-glycemic index carbohydrate increases nuclear factor-κB activation in mononuclear cells of young, lean healthy subjects. Am J Clin Nutr 2008;87:1188–1193.
[10] Chen PH, Chi JT, Boyce M. Functional crosstalk among oxidative stress and O-GlcNAc signaling pathways. Glycobiology 2018;28:556–564.
[11] Gentric G, Maillet V, Paradis V, Couton D, L'Hermitte A, Panasyuk G, et al. Oxidative stress promotes pathologic polyploidization in nonalcoholic fatty liver disease. J Clin Invest 2015;125:981–992.
[12] Bligh EG, Dyer WJ. A rapid method of total lipid extraction and purification. Can J Biochem Physiol 1959;37:911–917.
[13] Oliveros JC. Venny. An interactive tool for comparing lists with Venn's diagrams. 2007. 2015; https://bioinfogp.cnb.csic.es/tools/venny/index.html. [Accessed 13 October 2023].
[14] Blighe K, Rana S, Lewis M. EnhancedVolcano: publication-ready volcano plots with enhanced colouring and labeling. 2019; https://github.com/kevinblighe/EnhancedVolcano. [Accessed 13 October 2023].
[15] Kolde R. Pheatmap: pretty heatmaps R package version 1.0.12. 2019; https://CRAN.R-project.org/package=pheatmap. [Accessed 13 October 2023].
[16] Wang XJ, Hayes JD, Wolf CR. Generation of a stable antioxidant response element-driven reporter gene cell line and its use to show redox-dependent activation of Nrf2 by cancer chemotherapeutic agents. Cancer Res 2006;66:10983–10994.
[17] Guilbert T, Odin C, Le Grand Y, Gailhouste L, Turlin B, Ezan F, et al. A robust collagen scoring method for human liver fibrosis by second harmonic microscopy. Opt Express 2010;18:25794–25807.
[18] Park SK, Zhou X, Pendleton KE, Hunter OV, Kohler JJ, "Donnell KA, et al. A conserved splicing silencer dynamically regulates O-GlcNAc transferase intron retention and O-GlcNAc homeostasis. Cell Rep 2017;20:1088–1099.
[19] Baker NE. Emerging mechanisms of cell competition. Nat Rev Genet 2020;21:683–697.
[20] Aquilano K, Baldelli S, Ciriolo MR. Glutathione: new roles in redox signaling for an old antioxidant. Front Pharmacol 2014;5:196.
[21] Kalthoff S, Ehmer U, Freiberg N, Manns MP, Strassburg CP. Interaction between oxidative stress sensor Nrf2 and xenobiotic-activated aryl hydrocarbon receptor in the regulation of the human phase II detoxifying UDP-glucuronosyltransferase 1A10. J Biol Chem 2010;285:5993–6002.
[22] **Cho CS**, **Park HW**, Ho A, Semple IA, Kim B, Jang I, et al. Lipotoxicity induces hepatic protein inclusions through TANK binding kinase 1-mediated p62/sequestosome 1 phosphorylation. Hepatology 2018;68:1331–1346.
[23] Manley S, Williams JA, Ding WX. Role of p62/SQSTM1 in liver physiology and pathogenesis. Exp Biol Med (Maywood) 2013;238:525–538.
[24] Belmokhtar CA, Hillion J, Ségal-Bendirdjian E. Staurosporine induces apoptosis through both caspase-dependent and caspase-independent mechanisms. Oncogene 2001;20:3354–3362.
[25] Paradis V, Kollinger M, Fabre M, Holstege A, Poynard T, Bedossa P. *In situ* detection of lipid peroxidation by-products in chronic liver diseases. Hepatology 1997;26:135–142.
[26] Shmarakov IO, Jiang H, Liu J, Fernandez EJ, Blaner WS. Hepatic stellate cell activation: a source for bioactive lipids. Biochim Biophys Acta Mol Cell Biol Lipids 2019;1864:629–642.
[27] Pewzner-Jung Y, Park H, Laviad EL, Silva LC, Lahiri S, Stiban J, et al. A critical role for ceramide synthase 2 in liver homeostasis: I. alterations in lipid metabolic pathways. J Biol Chem 201;285:10902–10.
[28] Robarts DR, McGreal SR, Umbaugh DS, Parkes WS, Kotulkar M, Abernathy S, et al. Regulation of liver regeneration by hepatocyte O-GlcNAcylation in mice. Cell Mol Gastroenterol Hepatol 2022;13:1510–1529.
[29] Housley MP, Rodgers JT, Udeshi ND, Kelly TJ, Shabanowitz J, Hunt DF, et al. *O*-GlcNAc regulates FoxO activation in response to glucose. J Biol Chem 2008;283:16283–16292.
[30] **Geerts AM**, **Vanheule E**, Praet M, Van Vlierberghe H, De Vos M, Colle I. Comparison of three research models of portal hypertension in mice: macroscopic, histological and portal pressure evaluation. Int J Exp Pathol 2008;89:251–263.
[31] Lefebvre P, Staels B. Hepatic sexual dimorphism – implications for non-alcoholic fatty liver disease. Nat Rev Endocrinol 2021;17:662–670.
[32] Smati S, Polizzi A, Fougerat A, Ellero-Simatos S, Blum Y, Lippi Y, et al. Integrative study of diet-induced mouse models of NAFLD identifies PPARα as a sexually dimorphic drug target. Gut 2022;71:807–821.
[33] Roskams TA, Theise ND, Balabaud C, Bhagat G, Bhathal PS, Bioulac-Sage, et al. Nomenclature of the finer branches of the biliary tree: canals, ductules, and ductular reactions in human livers. Hepatology 2004;39:1739–1745.

[34] **Donne R**, **Saroul-Aïnama M**, **Cordier P**, Celton-Morizur S, Desdouets C. Polyploidy in liver development, homeostasis and disease. Nat Rev Gastroenterol Hepatol 2020;17:391–405.
[35] Yamaji S, Zhang M, Zhang J, Endo Y, Bibikova E, Goff SP, et al. Hepatocyte-specific deletion of DDB1 induces liver regeneration and tumorigenesis. Proc Natl Acad Sci USA 2010;107:22237–22242.
[36] **Zhang N**, **Bai H**, David KK, Dong J, Zheng Y, Cai J, et al. The Merlin/NF2 tumor suppressor functions through the YAP oncoprotein to regulate tissue homeostasis in mammals. Dev Cell 2010;19:27–38.
[37] Grindheim JM, Nicetto D, Donahue G, Zaret KS. Polycomb repressive complex 2 proteins EZH1 and EZH2 regulate timing of postnatal hepatocyte maturation and Fibrosis by repressing genes with euchromatic promoters in mice. Gastroenterology 2019;156:1834–1848.
[38] **Yanguas SC**, **Cogliati B**, Willebrords J, Maes M, Colle I, van den Bossche B, et al. Experimental models of liver fibrosis. Arch Toxicol 2016;90:1025–1048.
[39] Gilgenkrantz H, Mallat A, Moreau R, Lotersztajn S. Targeting cell-intrinsic metabolism for antifibrotic therapy. J Hepatol 2021;74:1442–1454.
[40] Rojas-Morales P, Pedraza-Chaverri J, Tapia E. Ketone bodies, stress response, and redox homeostasis. Redox Biol 2020;29:101395.
[41] Kolb H, Kempf K, Röhling M, Lenzen-Schulte M, Schloot NC, Martin S. Ketone bodies: from enemy to friend and guardian angel. BMC Med 2021;19:313.

Journal of Hepatology, Volume *6*

Supplemental information

O-GlcNAc transferase acts as a critical nutritional node for the control of liver homeostasis

Paula Ortega-Prieto, Lucia Parlati, Fadila Benhamed, Marion Regnier, Isadora Cavalcante, Mélanie Montabord, Rachel Onifarasoaniaina, Maryline Favier, Natasa Pavlovic, Julie Magusto, Michèle Cauzac, Patrick Pagesy, Jérémie Gautheron, Chantal Desdouets, Sandra Guilmeau, Tarik Issad, and Catherine Postic

O-GlcNAc transferase acts as a critical nutritional node for the control of liver homeostasis

Paula Ortega-Prieto, Lucia Parlati, Fadila Benhamed, Marion Regnier, Isadora Cavalcante, Mélanie Montabord, Rachel Onifarasoaniaina, Maryline Favier, Natasa Pavlovic, Julie Magusto, Michèle Cauzac, Patrick Pagesy, Jérémie Gautheron, Chantal Desdouets, Sandra Guilmeau, Tarik Issad, Catherine Postic

Table of contents

Supplementary figure legends.....2

Supplementary table legends.....6

Supplementary figures.....7

Supplementary tables.....16

Supplementary figure legends

Fig. S1. Physiological parameters in 4 week-old OGT^{LWT} and OGT^{LKO} mice. Male liver-specific *Ogt* knockout (OGT^{LKO}) and control floxed littermates (OGT^{LWT}) mice were studied 4 weeks after birth. **A.** Fasting blood glucose (5 hours) (mmol/L). **B**. Glucose tolerance test. The area under the curve (AUC) is shown. **C**. Pyruvate tolerance test. The area under the curve (AUC) is shown. **D**. Insulin tolerance test. The area under the curve (AUC) is shown. **E**. Western blot analysis of Foxo1 (whole lysate), Foxo1O-GlcNAcylation levels (WGA) and global O-GlcNAcylation in liver of OGT^{LWT} and OGT^{LKO} mice. Actin was used as loading control. Three representative samples are presented per condition. **F**. Relative expression levels of gluconeogenic genes normalized to TBP. Data are shown as Mean ± SEM of 6-8 male mice. *P < 0.05; **P < 0.01; ***P<0.001 by unpaired Student t-test (Mann-Whitney U test).

Fig. S2. Liver injury and cell identity assessment in OGT^{LKO} mice. Male liver-specific *Ogt* knockout (OGT^{LKO}) and control floxed littermates (OGT^{LWT}) mice were studied 8 weeks after birth in the fed state. **A**. Relative expression of *Oga* normalized to TBP **B**. Relative expression levels of proliferation markers normalized to TBP. **C**. Western blot analysis of proliferation markers. Three representative samples are shown. Actin was used as a loading control. **D**. Liver section of mice without macroscopic nodular phenotype stained with HE, Sirius red and OGT. **E**. Serum levels of aspartate aminotransferase (AST), total and direct bilirubin and alkaline phosphatase (ALP) in mice 8 weeks after birth. **F.** Representation of hepatoblast differentiation into hepatocytes or cholangiocytes. Markers used for cell characterization are represented under each cellular type. **G**. Relative expression of cell identity markers in livers from OGT^{LWT} compared to OGT^{LKO} mice at 4 and 8 weeks. TBP was used as a housekeeping gene. **H**. Liver sections of 8 week-old mice stained with HNF4α, SOX9 and

Krt19 antibodies. Scale bars = 100 μm on the two upper sections. Detailed zoom is shown in the bottom sections with a scale bar = 50μm. PV: Portal vein. CV: Central vein. Data are represented as Mean ± SEM of 8-10 mice at 4 weeks and 13-15 mice at 8 weeks. **P < 0.01; ***P < 0.001 by unpaired Student t-test (Mann-Whitney U test) comparing OGT^{LWT} and OGT^{LKO} at the same age (Panels A, B, E). **P <0.01; ***P <0.001 by two-way ANOVA followed by Bonferroni post hoc test (panel G).

Fig. S3. Female OGT^{LKO} mice exhibit severe liver damage.

Female liver-specific *Ogt* knockout (OGT^{LKO}) and control floxed littermates (OGT^{LWT}) mice were studied 8 weeks after birth in the fed state. **A**. Fed blood glucose (mmol/L), body (g), liver and spleen weights are shown. Liver and spleen weight are represented as percentage of body weight. **B**. Relative expression levels of *Ogt* normalized to TBP. **C**. Western blot analysis of OGT and CHOP protein content in liver of OGT^{LWT} and OGT^{LKO} mice. Four representative samples are shown. Actin was used as a loading control. **D**. Liver sections stained with hematoxylin-eosin (HE), Sirius red, αSMA, OGT, Ki67 and SOX9. Scale bars = 100 μm. **E**. Relative expression levels of inflammatory markers normalized to TBP. **F**. Relative expression levels of fibrosis markers normalized to TBP. **G**. Relative expression levels of oxidative stress markers normalized to TBP. **H**. Serum levels of alanine aminotransferase (ALT). Data are shown as Mean ± SEM of 5 female mice per condition. *P < 0.05; **P < 0.01; ***P < 0.001; ****P<0.0005 by unpaired Student t-test (Mann-Whitney U test).

Fig. S4. Heatmaps of oxidative stress, necroptosis, DNA repair and extracelular matrix.

A. Microarray results of genes involved in oxidative stress. **B**. Microarray results of genes involved in necroptosis. **C**. Microarray results of genes involved in DNA repair. **D**. Microarray results of significant changing genes involved in extracellular matrix formation. Genes found significantly different (either down or up-regulated) between OGT^{LWT} and OGT^{LKO} are

indicated by an asterisk (*). Differentially expressed (DE) gene cut-off was set for a fold change ≥ |2| and False discovery rate (FDR) p-value < 0.05.

Fig. S5. Kinetics of inflammation, oxidative stress and ER stress markers in liver of OGT^{LWT} and OGT^{LKO} mice. Male liver-specific *Ogt* knockout (OGT^{LKO}) and control floxed littermates (OGT^{LWT}) mice were studied 2, 4 or 8 weeks after birth in the fed state. **A**. Western blots showing protein content in whole liver lysates of inflammation (Phospho-JNK and total JNK), ER stress (CHOP) markers. Actin and/or HSP90 were used as loading controls. **B**. Relative expression levels of oxidative stress markers and of *Chop* normalized to TBP. Data are represented as Mean ± SEM of 6 mice per group age. *P < 0.05; ***P < 0.001; ****P < 0.0005 by two-way Anova followed by Bonferroni post hoc test.

Fig. S6. Persistent fibrosis and liver injury in 12 weeks and 12 months old OGT^{LKO} mice. Liver-specific *Ogt* knockout (OGT^{LKO}) and control floxed littermates (OGT^{LWT}) mice were studied 12 weeks and 12 months after birth in the fed state. **A.** Liver and spleen weights are shown and are represented as percentage of body weight. **B**. Relative expression levels of oxidative stress and inflammatory markers normalized to TBP. **C**. Liver sections stained with hematoxylin-eosin (HE) and F4/80. Scale bars = 100 μm. **D**. Serum levels of alanine aminotransferase (ALT) of alkaline phosphatase (ALP) and lactate dehydrogenase (LDH). Data are shown as Mean ± SEM of 18-20 individual male and female mice at 12 weeks and 12 months. *P < 0.05; **P < 0.01; ***P < 0.001 and ****P < 0.0005 by two-way ANOVA followed by Bonferroni post hoc test.

Fig. S7. Low carbohydrate high fat (LCHF) diet improves oxidative stress, ER stress and DNA damage but not fibrosis in OGT^{LKO} mice. A. Liver-specific *Ogt* knockout

(OGT^{LKO}) and control floxed littermates (OGT^{LWT}) mice were weaned (at 3 weeks of age) on a low carbohydrate high fat (LCHF in % of calories: 21% of carbohydrates, 60% of fat, 19% of proteins) diet and sacrificed 5 weeks later in the fed state. **B.** Body weight (g), liver and spleen weights are shown. Liver and spleen weights are represented as percentage of body weight. **C**. Serum concentrations of β-hydroxybutyrate. **D**. Relative expression levels of *Chop* normalized to TBP. **E**. Serum levels of Cxcl1. Data are shown as Mean ± SEM of 4-12 mice (males and females). *P < 0.05; ***P < 0.001; ****P< 0.0005 by two-way ANOVA followed by Bonferroni post hoc test.

Fig. S8. Ketogenic diet (KD) improves oxidative stress, ER stress, DNA damage, hepatic fibrosis and liver injury in OGT^{LKO} mice. A. Liver-specific *Ogt* knockout (OGT^{LKO}) and control floxed littermates (OGT^{LWT}) were weaned (at 3 weeks of age) on a ketogenic diet (KD: 1% of carbohydrates, 94% of fat, 5% of protein) and sacrificed 5 weeks later in the fed state. **B**. Body weight (g), liver and spleen weights are shown. Liver and spleen weights are represented as percentage of body weight. **C**. Serum concentrations of β-hydroxybutyrate**. D**. Relative expression levels of *Chop* normalized to TBP. Data are shown as Mean ± SEM of 4-8 mice (males and females). ***P < 0.001; ****P < 0.0005 by two-way ANOVA followed by Bonferroni post hoc test.

Fig. S9. Lipidomic analysis in liver of OGT^{LWT} and OGT^{LKO} mice fed on SD, LCHF or KD diets. A. Heat map of lipid species in liver from OGT^{LWT} and OGT^{LKO} mice fed at weaning for 5 weeks with a LCHF diet. Specific clusters are indicated. **B**. Heat map of lipid species in liver from OGT^{LWT} and OGT^{LKO} fed for 5 weeks at weaning with a KD diet. Specific clusters are indicated. Data are shown as Mean ± SEM of 4-12 mice (males and females).

Supplementary table legends

Table S1. Differentially expressed genes at 4 weeks

Table S2. Differentially expressed genes at 8 weeks

Table S3. Differentially expressed genes common to 4 and 8 weeks

Table S4. List of primers used for qPCR

Supplementary figures

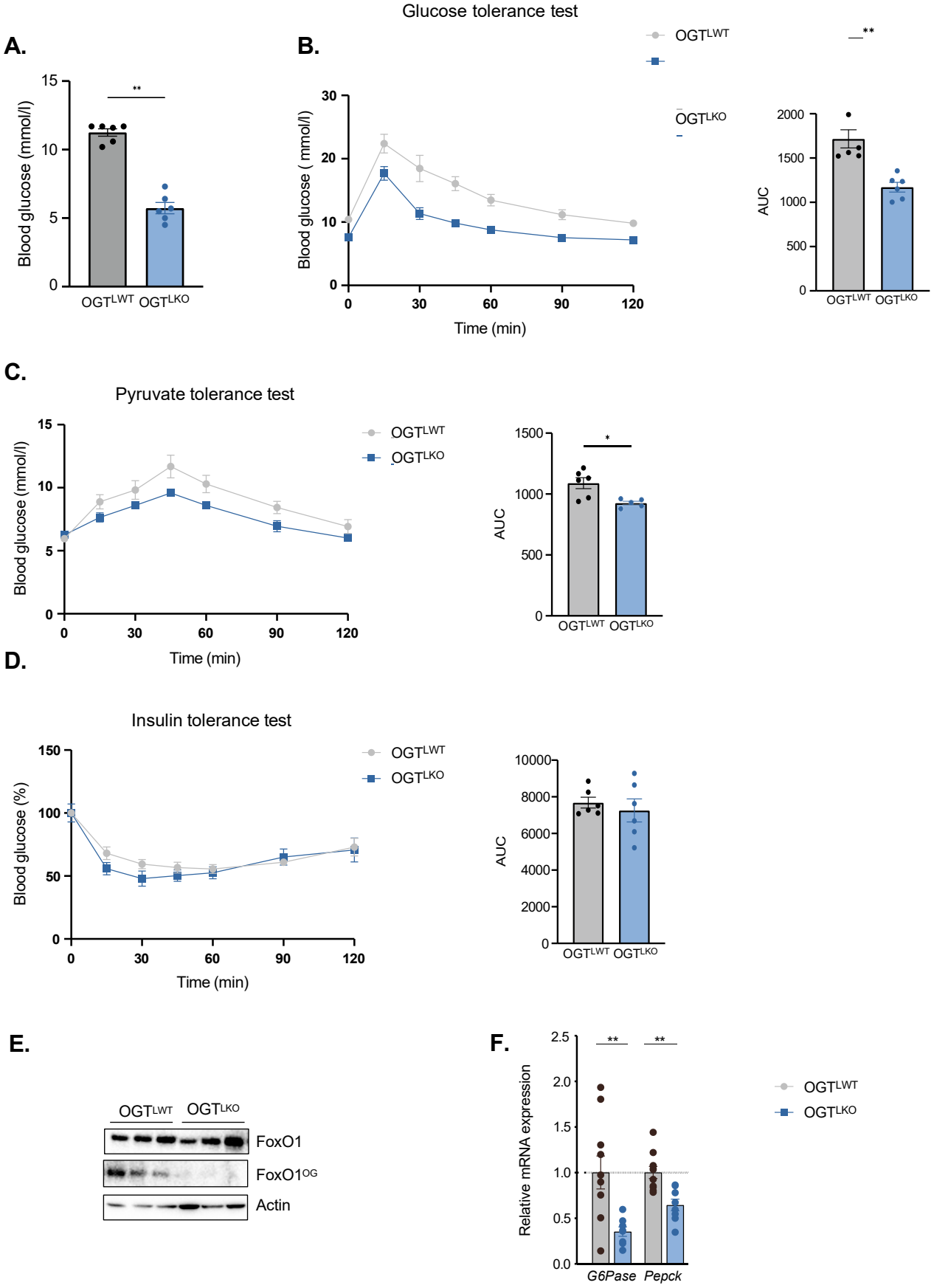

Fig. S1

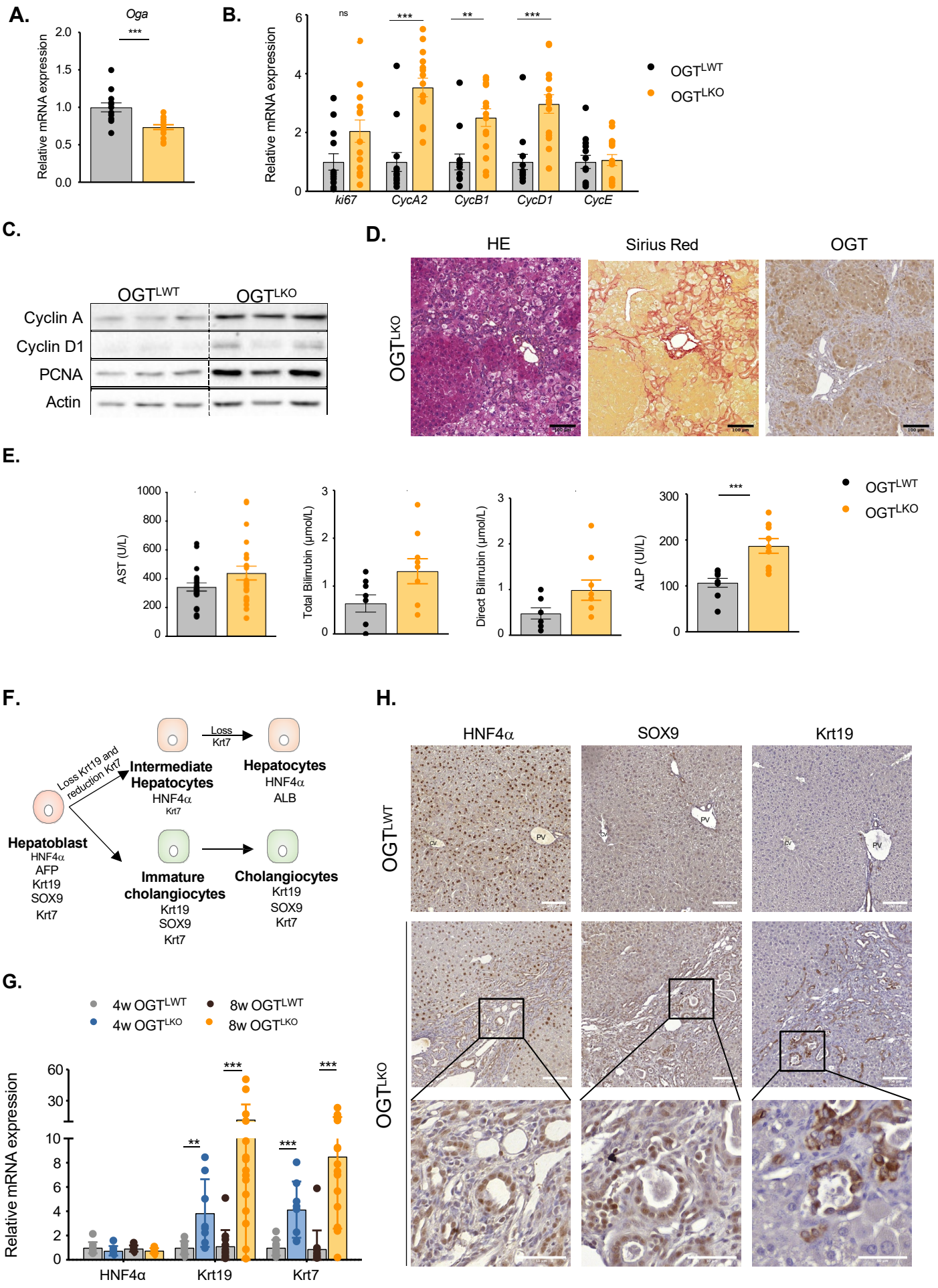
A.
Oga
***
Relative mRNA expression
2.0
1.5
1.0
0.5
0.0
B.
Relative mRNA expression
ns
***
**
***
ki67
CycA2
CycB1
CycD1
CycE
OGTLWT
OGTLKO
C.
OGTLWT
OGTLKO
Cyclin A
Cyclin D1
PCNA
Actin
D.
HE
Sirius Red
OGT
OGTLKO
E.
AST (U/L)
Total Bilirubin (μmol/L)
Direct Bilirubin (μmol/L)
ALP (UI/L)
***
OGTLWT
OGTLKO
F.
Loss Krt7
Loss Krt19 and reduction Krt7
Hepatoblast
HNF4α
AFP
Krt19
SOX9
Krt7
Intermediate Hepatocytes
HNF4α
Krt7
Hepatocytes
HNF4α
ALB
Immature cholangiocytes
Krt19
SOX9
Krt7
Cholangiocytes
Krt19
SOX9
Krt7
G.
4w OGTLWT
4w OGTLKO
8w OGTLWT
8w OGTLKO
Relative mRNA expression
HNF4α
Krt19
Krt7
H.
HNF4α
SOX9
Krt19
OGTLWT
OGTLKO
CV
PV

Fig. S2

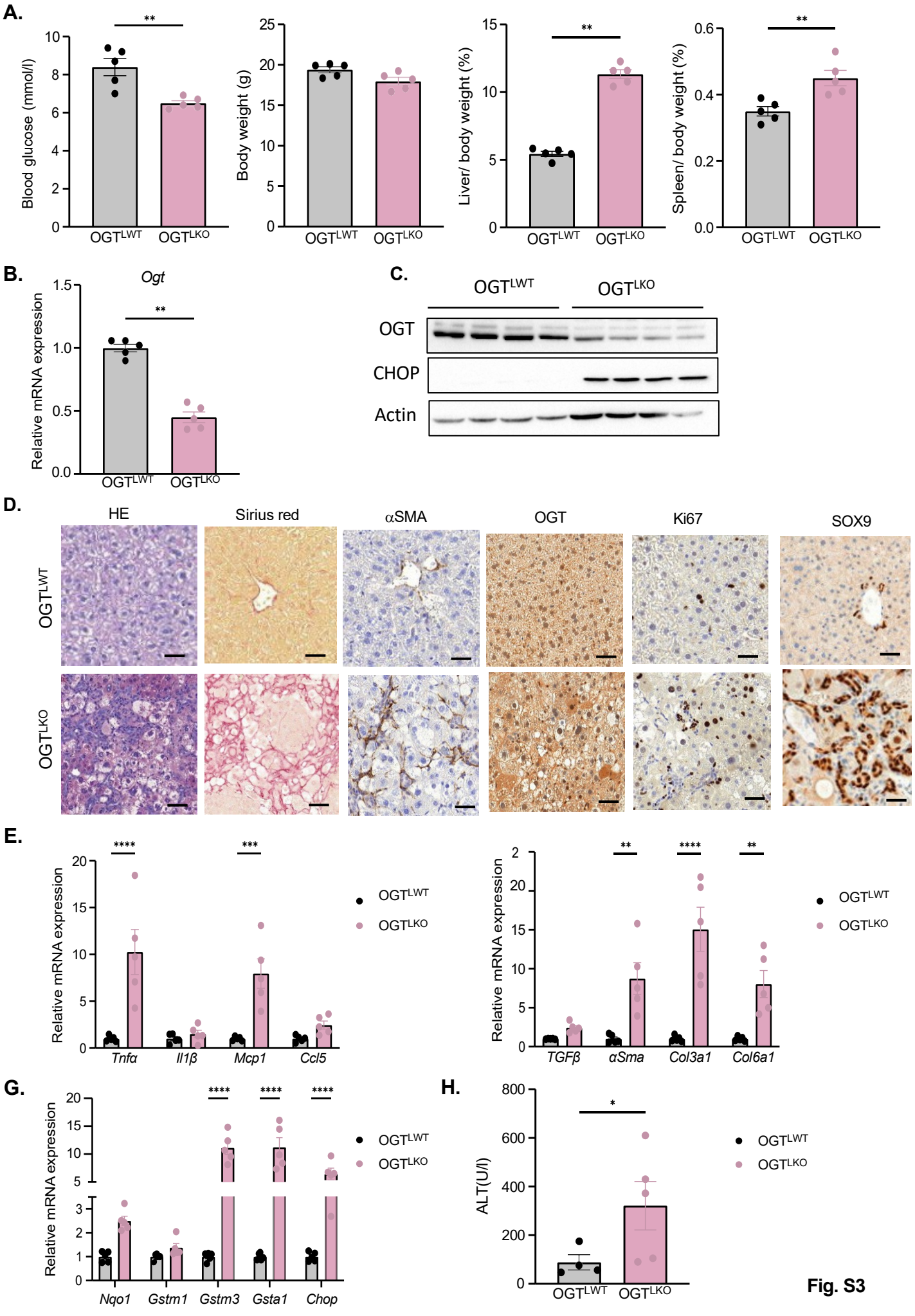
A.
Blood glucose (mmol/l)
Body weight (g)
Liver/ body weight (%)
Spleen/ body weight (%)
OGTLWT
OGTLKO
B.
Ogt
Relative mRNA expression
C.
OGT
CHOP
Actin
D.
HE
Sirius red
αSMA
OGT
Ki67
SOX9
E.
Relative mRNA expression
Tnfα
Il1β
Mcp1
Ccl5
TGFβ
αSma
Col3a1
Col6a1
G.
Nqo1
Gstm1
Gstm3
Gsta1
Chop
H.
ALT(U/l)

Fig. S3

A. Oxidative stress

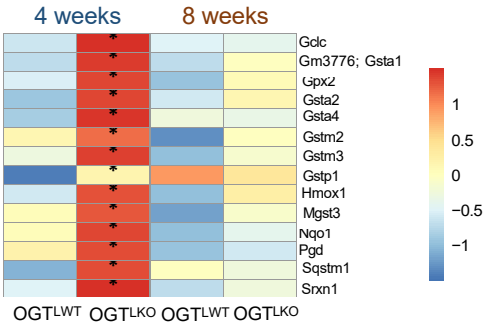

B. Necroptosis

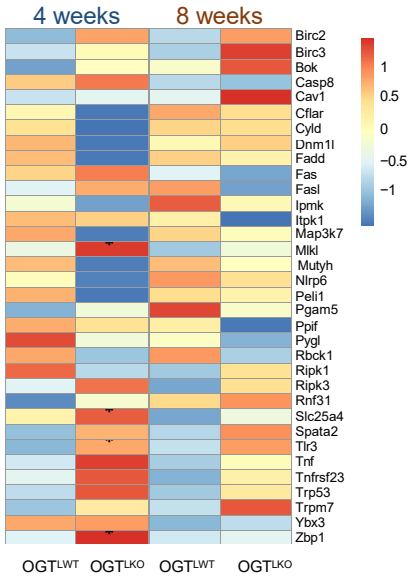

C. DNA repair

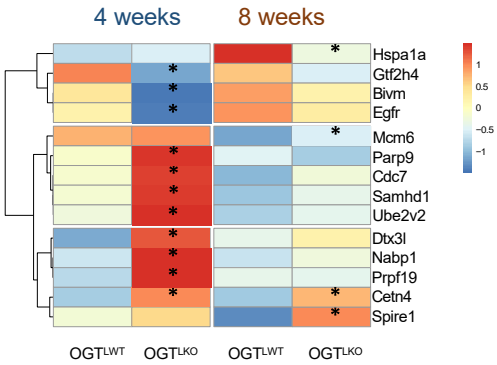

D. Extracellular matrix

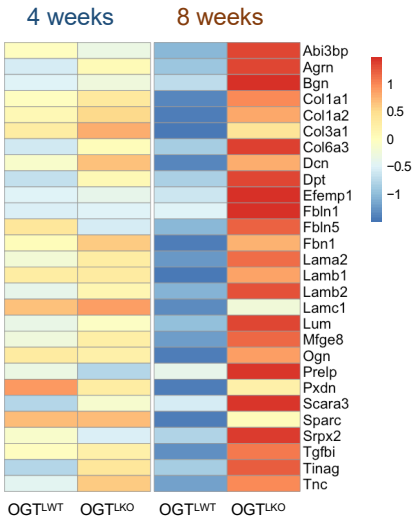

Fig. S4

A.

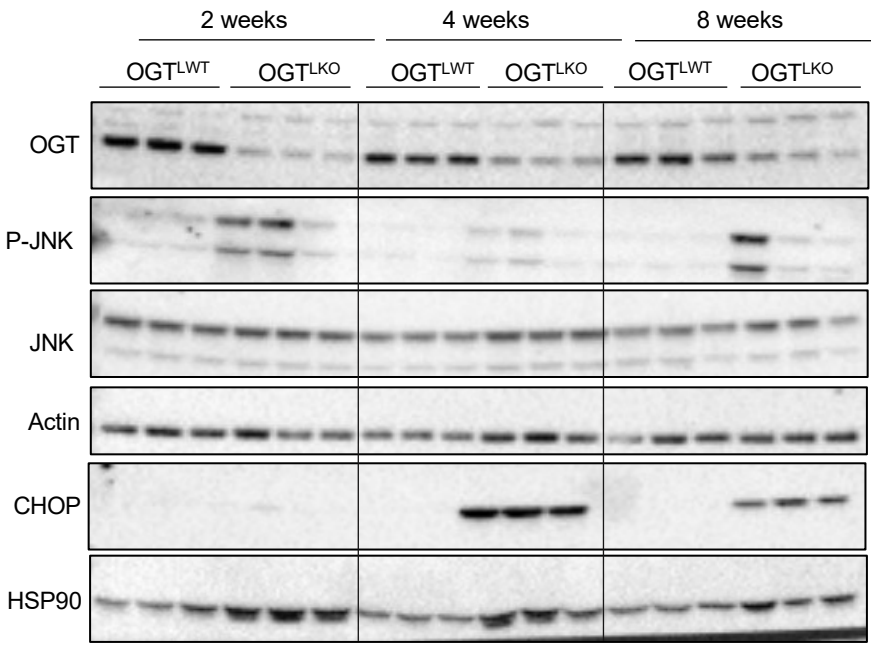
2 weeks
4 weeks
8 weeks
OGT^LWT
OGT^LKO
OGT^LWT
OGT^LKO
OGT^LWT
OGT^LKO
OGT
P-JNK
JNK
Actin
CHOP
HSP90

B.

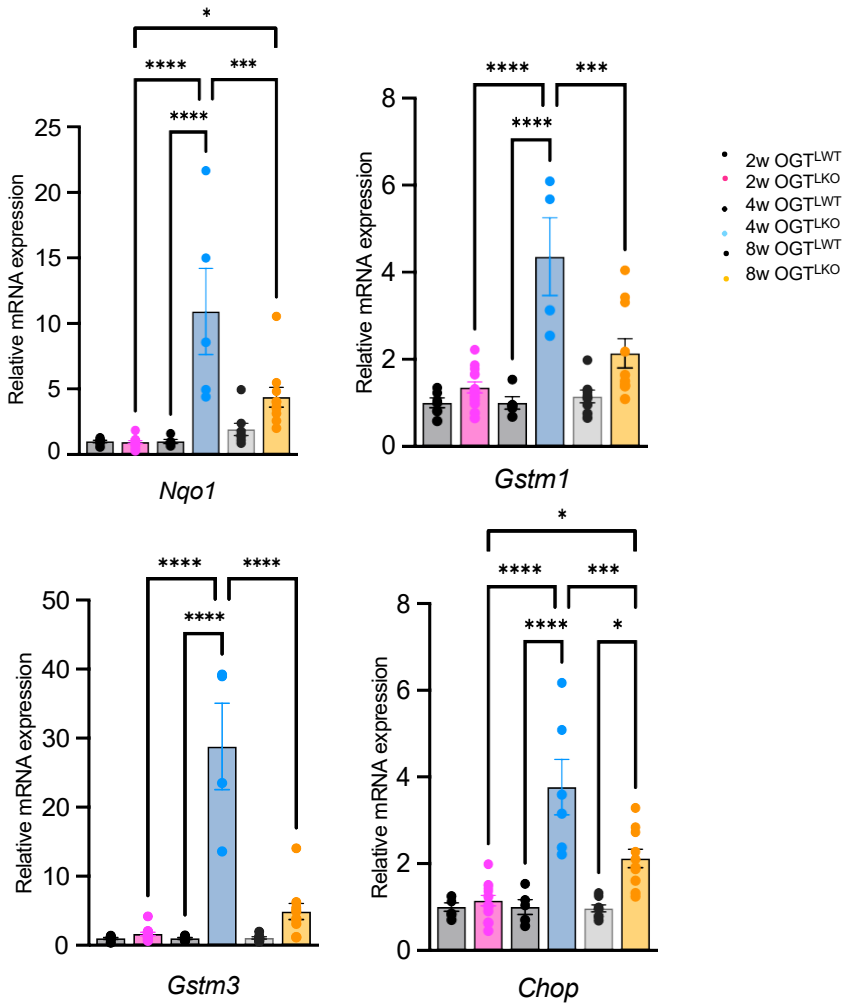
Relative mRNA expression
Nqo1
Gstm1
Gstm3
Chop
2w OGT^LWT
2w OGT^LKO
4w OGT^LWT
4w OGT^LKO
8w OGT^LWT
8w OGT^LKO

Fig. S5

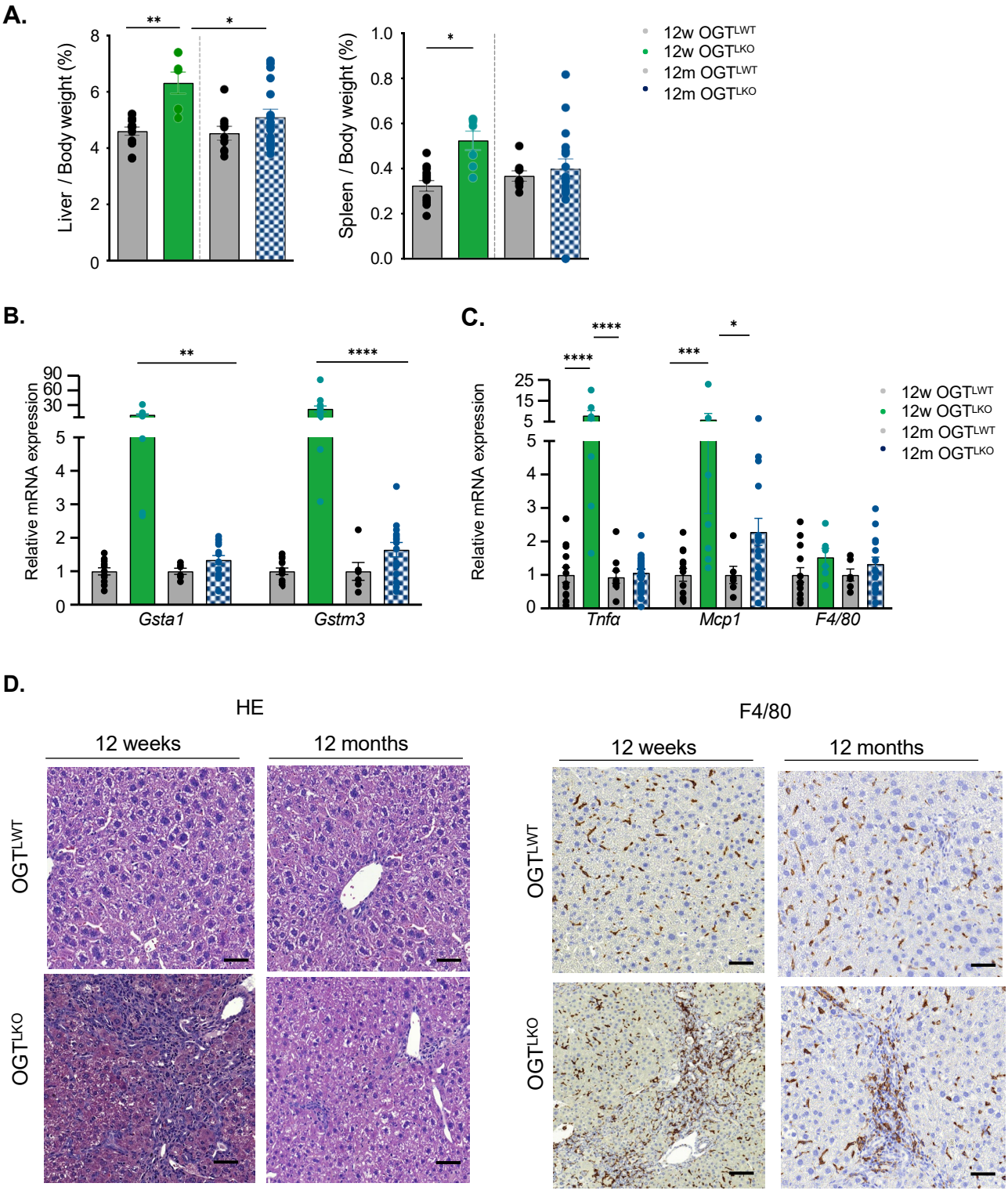
A.
Liver / Body weight (%)
Spleen / Body weight (%)
12w OGTLWT
12w OGTLKO
12m OGTLWT
12m OGTLKO
B.
Relative mRNA expression
Gsta1
Gstm3
C.
Relative mRNA expression
Tnfα
Mcp1
F4/80
D.
HE
F4/80
12 weeks
12 months
OGTLWT
OGTLKO
E.
ALT
ALP (UI/L)
LDH (UI/L)

Fig. S6

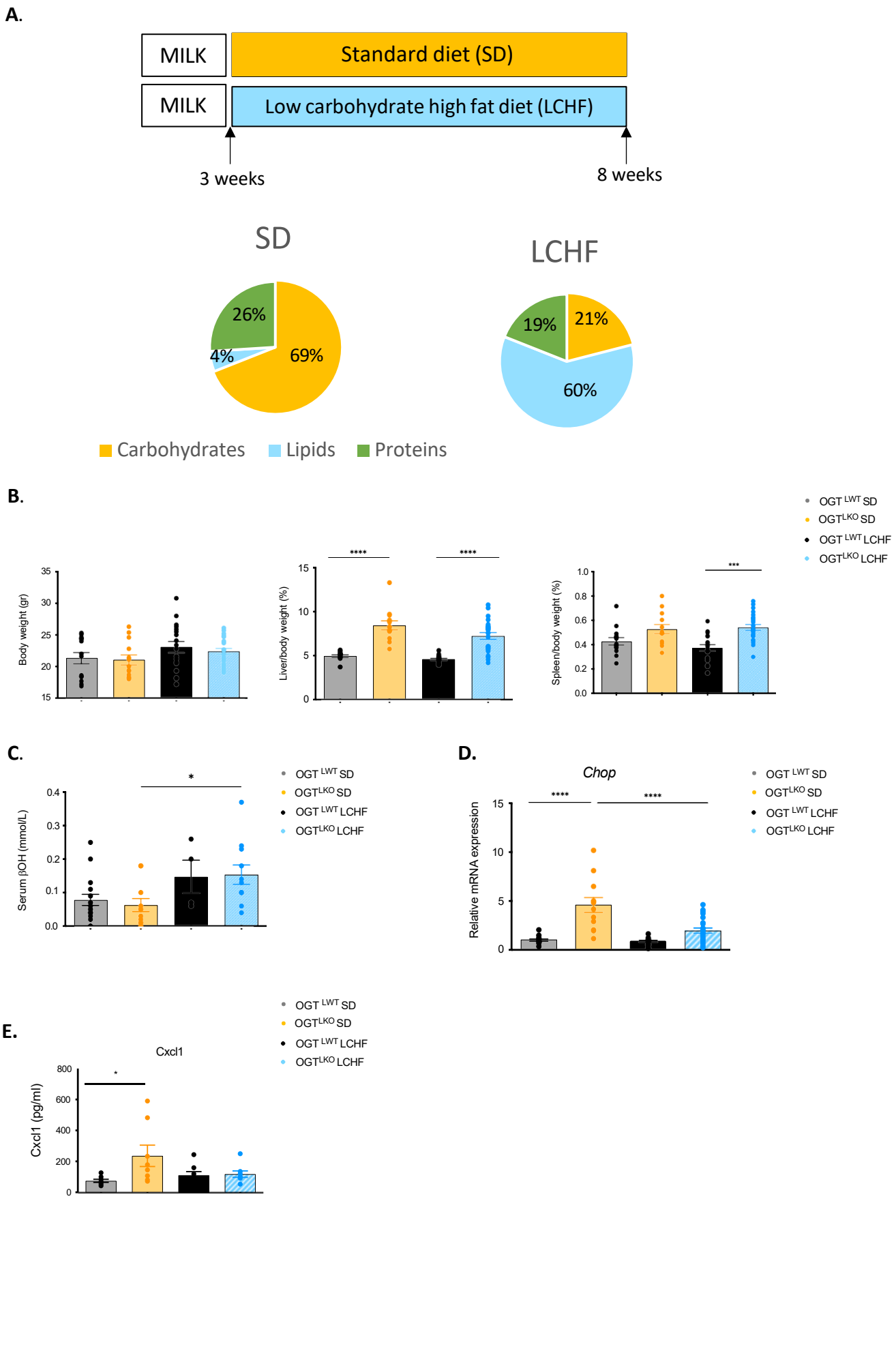
A.
MILK
Standard diet (SD)
MILK
Low carbohydrate high fat diet (LCHF)
3 weeks
8 weeks
SD
26%
4%
69%
LCHF
19%
21%
60%
Carbohydrates
Lipids
Proteins
B.
OGT LWT SD
OGTLKO SD
OGT LWT LCHF
OGTLKO LCHF
Body weight (gr)
Liver/body weight (%)
Spleen/body weight (%)
****
****
***
C.
Serum βOH (mmol/L)
*
D.
Chop
Relative mRNA expression
****
****
E.
Cxcl1
Cxcl1 (pg/ml)
*

Fig. S7

A.

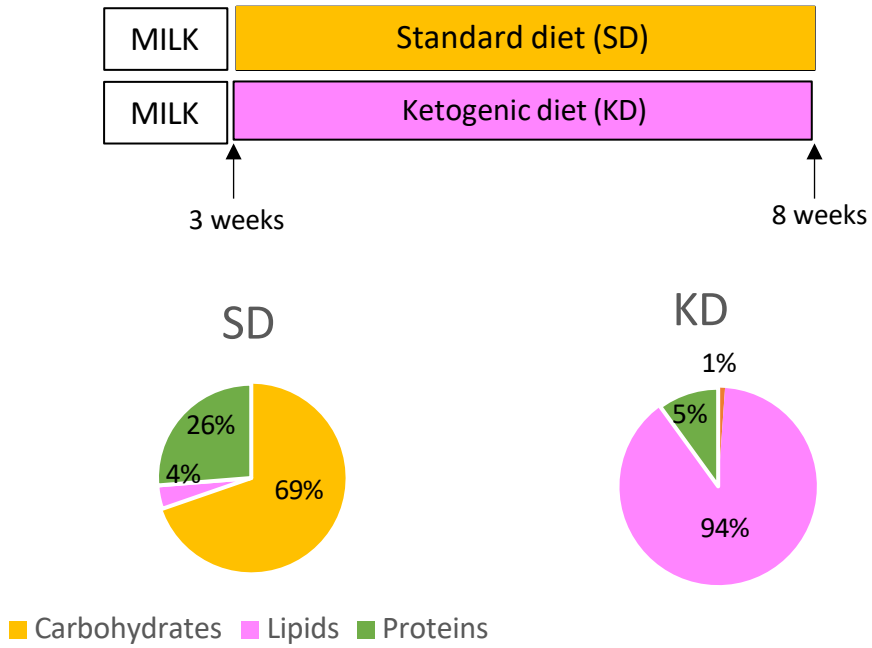
MILK
Standard diet (SD)
MILK
Ketogenic diet (KD)
3 weeks
8 weeks
SD
26%
4%
69%
KD
1%
5%
94%
Carbohydrates
Lipids
Proteins

B.

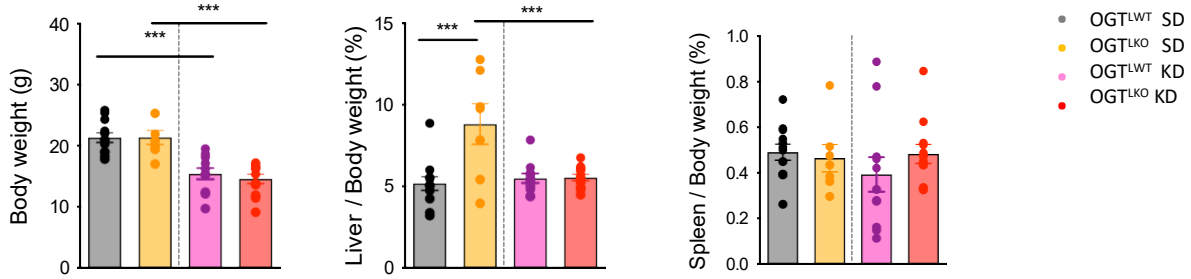
Body weight (g)
Liver / Body weight (%)
Spleen / Body weight (%)
OGTLWT SD
OGTLKO SD
OGTLWT KD
OGTLKO KD

C.

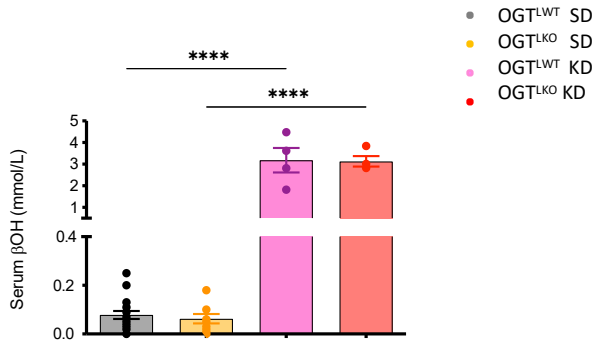
Serum βOH (mmol/L)
OGTLWT SD
OGTLKO SD
OGTLWT KD
OGTLKO KD

D.

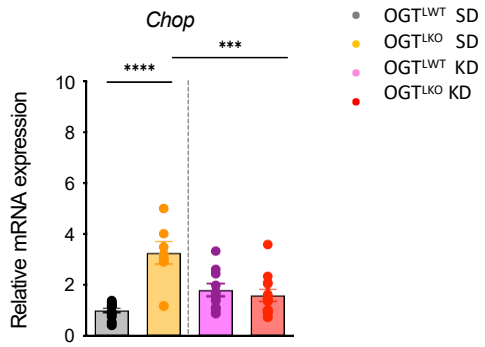
Chop
Relative mRNA expression
OGTLWT SD
OGTLKO SD
OGTLWT KD
OGTLKO KD

Fig. S8

A.

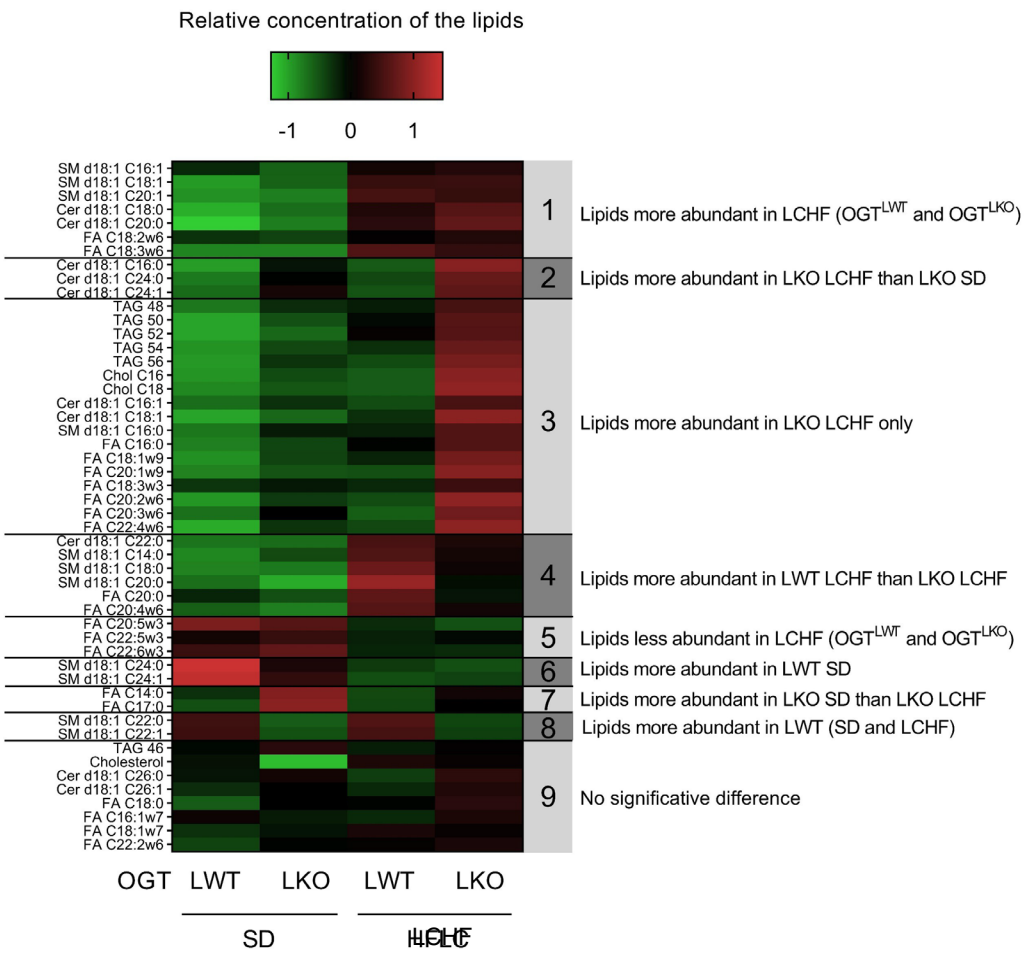
Relative concentration of the lipids
-1
0
1
SM d18:1 C16:1
SM d18:1 C18:1
SM d18:1 C20:1
Cer d18:1 C18:0
Cer d18:1 C20:0
FA C18:2w6
FA C18:3w6
Cer d18:1 C16:0
Cer d18:1 C24:0
Cer d18:1 C24:1
TAG 48
TAG 50
TAG 52
TAG 54
TAG 56
Chol C16
Chol C18
Cer d18:1 C16:1
Cer d18:1 C18:1
SM d18:1 C16:0
FA C16:0
FA C18:1w9
FA C20:1w9
FA C18:3w3
FA C20:2w6
FA C20:3w6
FA C22:4w6
Cer d18:1 C22:0
SM d18:1 C14:0
SM d18:1 C18:0
SM d18:1 C20:0
FA C20:0
FA C20:4w6
FA C20:5w3
FA C22:5w3
FA C22:6w3
SM d18:1 C24:0
SM d18:1 C24:1
FA C14:0
FA C17:0
SM d18:1 C22:0
SM d18:1 C22:1
TAG 46
Cholesterol
Cer d18:1 C26:0
Cer d18:1 C26:1
FA C18:0
FA C16:1w7
FA C18:1w7
FA C22:2w6
1
2
3
4
5
6
7
8
9
Lipids more abundant in LCHF (OGTLWT and OGTLKO)
Lipids more abundant in LKO LCHF than LKO SD
Lipids more abundant in LKO LCHF only
Lipids more abundant in LWT LCHF than LKO LCHF
Lipids less abundant in LCHF (OGTLWT and OGTLKO)
Lipids more abundant in LWT SD
Lipids more abundant in LKO SD than LKO LCHF
Lipids more abundant in LWT (SD and LCHF)
No significative difference
OGT
LWT
LKO
LWT
LKO
SD

B.

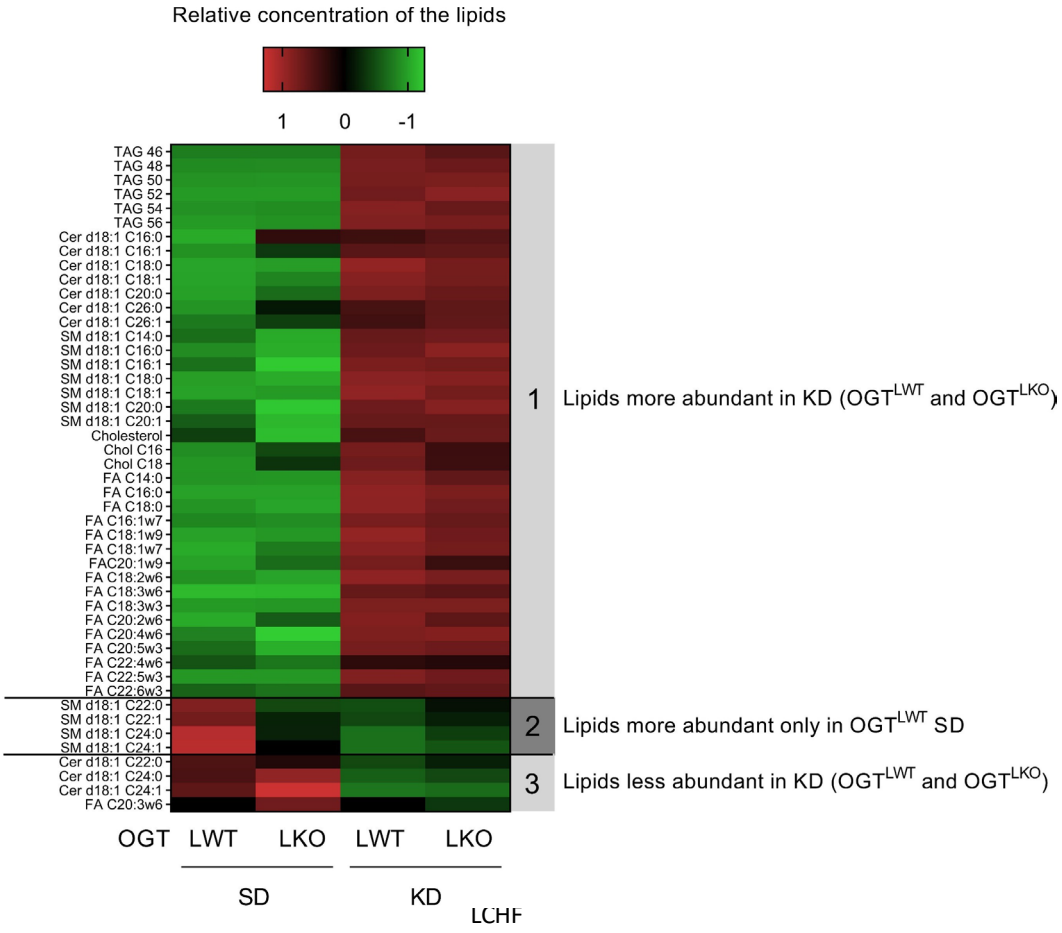
Relative concentration of the lipids
1
0
-1
TAG 46
TAG 48
TAG 50
TAG 52
TAG 54
TAG 56
Cer d18:1 C16:0
Cer d18:1 C16:1
Cer d18:1 C18:0
Cer d18:1 C18:1
Cer d18:1 C20:0
Cer d18:1 C26:0
Cer d18:1 C26:1
SM d18:1 C14:0
SM d18:1 C16:0
SM d18:1 C16:1
SM d18:1 C18:0
SM d18:1 C18:1
SM d18:1 C20:0
SM d18:1 C20:1
Cholesterol
Chol C16
Chol C18
FA C14:0
FA C16:0
FA C18:0
FA C16:1w7
FA C18:1w9
FA C18:1w7
FAC20:1w9
FA C18:2w6
FA C18:3w6
FA C18:3w3
FA C20:2w6
FA C20:4w6
FA C20:5w3
FA C22:4w6
FA C22:5w3
FA C22:6w3
SM d18:1 C22:0
SM d18:1 C22:1
SM d18:1 C24:0
SM d18:1 C24:1
Cer d18:1 C22:0
Cer d18:1 C24:0
Cer d18:1 C24:1
FA C20:3w6
1
2
3
Lipids more abundant in KD (OGTLWT and OGTLKO)
Lipids more abundant only in OGTLWT SD
Lipids less abundant in KD (OGTLWT and OGTLKO)
OGT
LWT
LKO
LWT
LKO
SD
KD

Fig. S9

Supplementary tables

Table S1. DE genes at 4 weeks.

0610010F05Rik	C6	Dhx38	Gcdh
0610011F06Rik	Calml4	Dhx58	Gclc
1110012L19Rik	Car5a	Dixdc1	Gcsh
1700001C19Rik	Car5b	Dlg3	Gde1
1700024P16Rik	Cbr1	Dnaic1	Gdpd1
1810011O10Rik	Cbr3	Dnajc2	Gipc2
2010003K11Rik	Ccbl1	Dnajc4	Gm10639
9130409I23Rik	Ccdc120	Dnpep	Gm10768; Abcc2
A1bg	Ccl19	Dnttip2	Gm11437
Abca3	Ccl2	Dpm3	Gm13139; Znf41-ps
Abcb8	Ccrl2	Dpyd	Gm13248
Abhd14b	Cd200r1	Dtx3l	Gm13251
Abhd15	Cd5l	Dusp10	Gm18853
Abhd6	Cdc7	Dynll1	Gm1966
Acad12	Cdk11b	Ear12; Ear2; Ear3	Gm2a
Acot1	Cdkl5	Echdc1	Gm3776; Gsta1
Acot3	Cenpp	Eda2r	Gm4794
Acot4	Ces1d	Eif2ak2	Gm4952
Acsl1	Ces1e	Eif2d	Gm4955
Acss2	Ces1f	Eif6	Gm7120
Adar	Ces3b	Elovl3	Gm8074
Adgrf1	Cidec	Elp4	Gpi1
Adra1b	Cisd1	Emc10	Gpr155
Afm	Cldn12	Enox2	Gpr35
Afp	Clec2d	Enpep	Gpt
Agpat5	Clpb	Entpd5	Gpx2
AI464131	Cmbl	Epas1	Grb7
Aida	Cmpk2	Epb41l4b	Grem2
Akr1c12	Cmtm6	Ephx1	Gsta2
Akr1c13	Cnnm2	Epsti1	Gsta4
Akr1c19	Cnpy2	Etfdh	Gstk1
Aldh6a1	Coa3	F11	Gsto1
Aph1c	Cops7b	Fabp5	Gstp1
Apol9a	Cox19	Fam131c	Gstp2
Apol9b	Crip2	Fam20a	Gstt1
Apom	Cryz	Fam210b	Gstt3
Apon	Cxcl10	Fam60a	Gtf2h4
Arhgap6	Cxcl9	Fam98a	Gtf2ird2
Arrdc4	Cyp2a22	Fastkd2	Guf1
Aspdh	Cyp2a5; Cyp2a4	Fbxo36	Gvin1
Aspg	Cyp2c40	Fbxo4	Gzmd; Gzme
Asrgl1	Cyp2c69	Fcgrt	H2-Ke6

Atat1	Cyp2d37-ps	Fetub	H2-L; H2-D1
Atf3	Cyp2f2	Fgf21	H2-Q1
Atp2b2	Cyp2j5	Fgfr4	H2-Q4
Atp5e	Cyp2u1	Fhit	H2-Q5
Atp6v1d	Cyp4a31	Foxo1	H2-Q7; H2-Q9
B4galnt1	Cyp4a32	Foxp1	H2-Q8; H2-Q6
Bax	Cyp4f15	Ftsj3	H2-T10
BC021614	Cyp4f17	Fzd8	H2-T22; H2-T9
BC089597	Dapk1	Gabrb3	Hacl1
Bcl2a1a	Dbt	Galnt10	Hao2
Bcl2a1d	Dcxr	Galnt4	Hcfc1r1
Bivm	Ddit3	Gamt	Heatr1
Bmp1	Ddx58	Gbp10; Gbp6	Herc6
Bmp8b	Ddx60	Gbp11	Hes6
Bnip3	Decr2	Gbp2b; Gbp5	Hgfac
Borcs8	Defb1	Gbp3	Hint2
Bphl	Dhx33	Gbp4	Hmox1
Brix1	Dhx37	Gbp9	Hn1

Hpn
Hps4
Hs3st3b1
Hsbp1l1
Hsd11b1
Hsd17b7
Hsd3b1
Hspb1
Hspbap1
Htra2
Hykk
Ifi35
Ifi44
Ifih1
Ifit1
Ifit1bl1
Ifit2
Ifit3
Ifit3b
Igfals
Il22ra1
Il2rg
Impact
Inmt
Irak1; Mir718; Mir5132
Irf7
Irs2
Isg15
Isoc2a
Itih1
Ivd
Kdelc1
Kif3a
Kitl
Klf12
Klf9
Klk1b4
Klkb1; Cyp4v3
Kptn
Krt18
Krt20
Krt8
Mb21d1
Mccc2
Mest
Mgam
Mgea5
Mgll
Mitd1
Mlkl
Mlxipl
Mmab
Mmachc
Mmp13
Mndal
Mpst
Mpv17l2
Mrpl24
Mrpl34
Ms4a4b
Ms4a6b
Msmo1
Mterf3
Mup-ps19; Mup20
Mup20
Mut
Mx1
Mx2
Myc
Myo5c
Myo6
N4bp2
Nabp1
Naglu
Nampt
Ncald; Gm15941
Ndufa3
Ndufaf3
Ndufv3
Neto2
Nit2
Nop56; Snord57
Nqo1
Nr1i3
Pak1ip1
Pank1
Papss2
Paqr9
Parp12
Parp14
Parp9
Pbld1
Pcca
Pccb
Pcid2
Pde9a
Pdk1
Pdxk
Pecr
Peg10
Pex7
Pfdn2
Pgd
Phf11a
Phf11b
Phkg2
Phyhd1
Pik3c2g
Pkd2l2
Pklr
Plek
Pm20d1
Pmvk
Pnpo
Polr3g
Ppfibp2
Ppm1k
Prkra
Prlr
Prodh2
Prpf19
Prpsap1
Prr14
Prss8
Prune
Psmb8
Rars
Rbbp9
Rdh11
Rdh16
Reep6
Rfc2
Rgs1
Rhoc
Rhod
Rnf213
Rnf34
Rock2
Rpn2
Rsad2
Rtp4
Saa3
Samhd1
Scap
Scnn1a
Sec11c
Sell
Selo
Sema4g
Serf1
Serpine2
Serpinf1
Serpinf2
Sesn3
Sfxn1
Sfxn5
Sgsm1
Shb
Shmt1
Slc10a5
Slc11a1
Slc15a3
Slc16a10
Slc16a12
Slc16a2
Slc20a1
Slc22a28
Slc22a30
Sp4
Spats2
Sqle
Sqstm1
Srd5a2
Srxn1
Sstr2
St6galnac6; St6galnac4
Stab2
Stard4
Stat2
Steap2
Stx2
Sult2a8
Sult3a1
Suox
Tcp11l2
Tesk2
Tfdp2
Thoc6
Thtpa; Zfhx2os
Timm21
Tlcd2
Tlr1
Tlr2
Tlr3
Tm2d2
Tmem184c
Tmem256
Tmem43
Tmem53
Tmem97
Tmprss2
Tnfrsf12a
Tnfsf10
Tor1b
Tor3a
Tox
Tprkb
Trim30a
Trim34b; Trim34a
Trmt10a

Lage3	Nr5a2	Psmd5	Slc25a23	Tsc22d3
Lgals3bp	Nrg1	Psmd8	Slc25a42	Tsku
Lilr4b	Nt5dc1	Ptcd3	Slc25a51	Ttc36
Lin7a	Nt5e	Pter	Slc29a1	Ttc38
Lmf1	Nudt19	Ptgr1	Slc35b4	Ttll7
Lonp1	Nudt2	Ptprc	Slc35c2	Uap1l1
Lrp11	Nup133	Pvr	Slc35d1	Ube2v2
Lrrc3	Nup62cl	Pwp2	Slc35e3	Ugdh
Lrsam1	Nxt2	Pxmp2	Slc44a1	Ugp2
Lsg1	Oaf	Pxmp4	Slc47a1	Ugt2a3
Ly6a	Oas1a	Pydc3	Slc4a7	Ugt3a1
Ly6c1	Oas1g	Pydc4	Slc6a12	Ugt3a2
Ly6c2	Oasl2	Pygo1	Slfn5	Ulk2
Lyar	Odf3b	Pyhin1	Slfn8	Uqcr10
Mafb	Ogfrl1	Qdpr	Slpi; Mir7678	Urm1
Man2b2	Ogt	Qsox1	Snrpa1	Uroc1
Map2k6	Orm1	Rab11fip2	Sox6	Usp18
Marchf2	Pafah2	Rabac1	Sp100	Vps28

Vps51; Tm7sf2
Vwa8
Wfdc2
Wfdc21
Wfdc3
Xaf1
Xdh
Yeats4
Yif1a
Zbp1
Zcchc24
Zcwpw1
Zfand4
Zfp65
Zfp729a
Zfp729b
Zpr1

Table S2. DE genes at 8 weeks.

1600002H07Rik	Atp8a1	Clstn1	Epha3	Gpm6a	Klf6
1700011H14Rik	Axl	Cmtm3	Epha7	Gpm6b	Klhl13
1700047I17Rik2	B4galt6	Cmtm3	Ephx4	Gpr65	Krt19
2210013O21Rik	Bambi	Col1a1	Erich5	Gpx3	Krt7
2610305D13Rik	Bcam	Col1a2	Etl4	Gsn	Lama2
6720489N17Rik	Bcl2	Col3a1	Ets2	Gstm2	Lamb1
Aadat	Bgn	Col6a3	Ezr	Gucy1a3; Mir7010	Lamb2
Abcd2	Bicc1	Cox18	Fam105a	H2-Ab1	Lamc1
Abhd2	C1qb	Cptp	Fam107a	H2-DMb1	Lbh
Abi2	C1qc	Creb3l1	Fam177a	H2-M2	Ldb1
Abi3bp	C1qtnf7	Crtap	Fam180a	Heph	Ldhd
Abr	C3ar1	Csf1r	Fam19a2	Hexa	Lgi2
Ace	Cacnb3	Csrp1	Fam205a2	Hexb	Lgmn
Acot9	Cadm4	Ctgf	Fam47e	Hgf	Lhfp
Acsf2	Capn8	Ctsk	Fbln1	Hist1h2ak	Loxl1
Actg1; Mir6935	Car2	Cttnbp2nl	Fbln5	Hnf4g	Loxl2
Adamts1	Casc4	Cxcr4	Fbn1	Hnrnpa1	Lpar1
Adamts2	Casp12	Cygb	Fcgr3	Hpgds	Lpl
Adamts5	Cav2	Cyp7b1	Fcna	Hsd3b4	Lrrcc1
Adamts9	Cbx6	Cyp8b1	Fermt1	Hsd3b4	Ltbp4
Adamtsl2	Ccdc3	Cysltr1	Fgfr3	Htra1	Lum
Add1; Mir7036b	Ccdc80	D17H6S56E-5	Fgl2	Icosl	Ly86
Adgre5; Mir1668	Ccdc88a	Dab2	Fhl2	Idh2	Lyz2
Adgrg1	Ccnd1	Dcdc2a	Flrt2	Ifi27l2a	Macc1
Adgrg6	Cd14	Dcn	Fmo2	Ifi27l2b	Mamdc2
Adh6-ps1	Cd163	Ddah2	Foxq1	Ifi30	Mamld1
Aebp1	Cd24a	Ddit4l	Frzb	Ifngr1	Map3k1
Agpat4	Cd300lh	Ddr2	Fut10	Ift57	Map4k4
Agrn	Cd300lh	Ddx26b	Fxyd5; Mir7050	Igf1r	Marcks
Ahnak; Mir6367	Cd34	Dkk3	Fzd1	Igfbp3	Mark1
AI506816	Cd36	Dnal1	G2e3	Igfbp7	Mbnl3
Aldh1a2	Cd52	Dock10	G6pdx	Ikbip	Mboat1
Angpt1	Cd68	Dpt	Gabra3	Il10rb	Mcm6
Ankrd1	Cd74; Mir5107	Dpy19l3	Gabrp	Islr	Meis2
Ano1	Cdh6	Dpysl2	Galnt3	Itga3	Mfge8
Ano6	Cdk14	Efemp1	Gas6	Itga8	Mgat4a
Antxr1	Cerk	Efhd2	Gdf10	Itga9	Mid1
Anxa13	Chchd7	Efnb2	Gem	Itgb5	Mir3962
Anxa2	Chst15	Egflam	Gfpt2	Itgb6	Mir6950
Anxa3	Cib3	Ehd2	Gja1	Itgb8	Mir7025
Aoah	Clca3a1; Clca1	Ehf	Gldn	Itgbl1	Mir7677
Apobec3	Clca3a2; Clca2	Elf4	Gm10052	Itm2c	Mmp14

App	Cldn4	Emb	Gm10600	Itpr3	Mmp2
Arg2	Cldn7	Emp1	Gm11710	Itpripl2	Moxd1
Arhgdib	Cldn8	Emp2	Gm11711	Jag1	Mrc2
Arhgef6	Clec4n	Emp3	Gm11711	Jchain	Ms4a4a
Arpc1b	Clic1	Eng	Gm609	Kalrn	Ms4a4d
Art4	Clic6	Enho	Gng2	Kcnma1	Muc1
Atp2b4; Mir6903	Clmp	Enkur	Golm1	Kifc3	Mxra8
Atp6v0d2	Cln6	Epcam	Gpc3	Klf5	Myadm

Mybl1	Pcdhgc3	Rbl1	Tmem229b
Myh9	Pcdhgc4	Rbm3	Tmem45a
Myo1d	Pcdhgc5	Rbms1	Tmem47
Myo7a	Pde1a	Rbms3	Tmsb10
Nav1	Pdgfc	Rbp1	Tmsb4x
Ncam1	Pdgfd	Rcn1	Tnc
Ncoa7	Pdgfra	Rgs2	Tnfrsf19
Ndrg1	Pdgfrb	Rhob	Tns1
Nedd9	Pdzk1ip1	Rhoj	Tns3
Nek5	Pea15a	Rnasel	Tox3
Ngfrap1	Pear1	Robo1	Tpm4
Nipal1	Phactr2	Robo2	Tpr
Nipal2	Phlda1	Rragd	Trib1
Nmnat1	Phldb2	Rtn4	Trove2
Nox4	Pirb	S100a11	Tspan3
Npcd	Pisd-ps3	Scara3	Tspan8
Npr2	Pkd2	Scarf2	Ttc3
Nptxr	Pkhd1	Sccpdh	Tuba1a
Nt5c3b	Plat	Scd2; Mir5114	Ucp2
Nudt7	Pld4	Sdr9c7	Ugt2b38
Obp2a	Plekha2	Selenbp2	Unc5b
Ogn	Plekho1	Selm	Veph1
Olfml3	Plet1	Selplg	Vgll3
Osmr	Plk2	Sema3c	Vim
Pacs1	Plod2	Sema3f	Wbp5
Pam	Plp2	Sema5a	Wfdc15b
Pamr1	Plxdc2	Sema6a	Wls
Parm1	Plxna4	Septin11	Wwc2
Parp8	Ppic	Septin8	Zeb2; Mir5129
Pawr	Ppp1r9b	Serpinb6a	
Pbk	Prelp	Serpinh1	
Pcdhga1	Prex2	Sestd1	
Pcdhga10	Prkch	Sftpd	
Pcdhga11	Prom1	Sh2d4a	
Pcdhga12	Prr15l	Sh3kbp1	
Pcdhga2	Prrg1	Tgfb2	
Pcdhga3	Ptger4	Tgfb3	
Pcdhga4	Ptgfrn	Tgfbi	
Pcdhga5	Ptpn13	Thbs1	
Pcdhga6	Ptpn14	Thbs2	
Pcdhga7	Ptprm	Tiam2	
Pcdhga8	Ptprs	Timp2	

Pcdhga9	Pxdn	Timp3
Pcdhgb1	Rab27b	Tinag
Pcdhgb2	Rab31	Tlr4
Pcdhgb4	Rab8b	Tlr7
Pcdhgb5	Ralgds	Tm4sf1
Pcdhgb6	Rarres1	Tmem106a
Pcdhgb7	Rasef	Tmem173
Pcdhgb8	Rassf9	Tmem189

Table S3. DE genes common to 4 and 8 weeks.

9230110C19Rik	Ifi204
9930111J21Rik1; 9930111J21Rik2	Ifi27
9930111J21Rik2	Iqgap1
Abcb1a	Laptm5
Adora1	Lenep; Flad1
Aebp2	Lifr
AI607873	Lilrb4a
Ajuba	Ly6e
Alcam	Mgst3
Anxa5	Mmp12
Bcl2a1b; Bcl2a1a	Mnda
Capsl	Mpv17l
Ccl22	Ms4a4c
Ccr2	Ms4a6c
Cd180	Ms4a6d
Cd44	Ms4a7
Cd53	Myl12a
Cd63	Myof
Cd9	Nid1
Cetn4	Npnt
Chic1	Ntrk2
Clec12a	P2ry4
Clec7a	Pafah1b3
Csprs	Phf11d; Phf11c
Ctss	Pla2g7
Cxcl16	Plac8
Cybb	Plekhb1
Elovl7	Pygb
Epb41l4a	Retsat
Evi2a; Evi2b; Gm21975	Samd9l
F2rl1	Septin6
Fads3	Sirpa
Fgf1	Slamf7
Flna	Slamf9
Fn3krp	Slc22a26
Glipr1	Slc25a45
Gm13212	Slfn2
Gm2399	Spi1
Gm3934	Tceal8
Gm5431	Tcf24
Gm9844	Tlr13
Gpnmb	Tmem176b

Gstm3
H2-Aa
H2-DMb2
H2-Eb1
Haus8
Hcls1
Ido2
Ifi203
Tmem19
Tnfaip3
Vcam1

Table S4. Primer sequences.

Name	Sequence
Ccl5 F	CTG ACC CTG TAT AGC TTC CCT
Ccl5 R	GGG ATT ACT GAG TGG CAT CC
Chop F	AAG GAG AAG GAG CAG GAG AAC
Chop R	GGT ACA CTT CCG GAG AGA CAG
Col3a1 F	CTGTAACATGGAAACTGGGGAAA
Col3a1 R	CCATAGCTGAACTGAAAACCACC
Col6a1 F	CTGCTGCTACAAGCCTGCT
Col6a1 R	CCCCATAAGGTTTCAGCCTCA
CycA2 F	TGC CTT CAC TCA TTG CTG GA
CycA2 R	TGT GGC GCT TTG AGG TAG GT
CycB1 F	TGC CTT TGT CAC GGC CTT AG
CycB1 R	GGA AAT TCT TGA CAA CGG TG
CycD F	GCG TAC CCT GAC ACC AAT CTC
CycD R	CTC CTC TTC GCA CTT CTG CTC
CycE F	CAGAGCAGCGAGCAGGAGA
CycE R	CAGCTGCTTCCACACCACTG
F4/80 F	CTT TGG CTA TGG GCT TCC AGT C
F4/80 R	GCA AGG AGG ACA GAG TTT ATC GTG
Gpx3 F	GCC ATT TGG CTT GGT CAT TC
Gpx3 R	TGG GGA GTA TCT CCG AGT TC
Gpx4 F	GCA CGA ATT CTC AGC CAA GG
Gpx4 R	CAA ACT GGT TGC AGG GGA AG
Gclc F	CTG CAC ATC TAC CAC GCA GT
Gclc R	TTC ATG ATC GAA GGA CAC CA
Gss F	GAAGCAGCTCGAAGAACTGG
Gss R	AGCACTGGGTACTGGTGAGG
Gsta1 F	CCA GAG CCA TTC TCA ACT A
Gsta1 R	TGC CCA ATC ATT TCA GTC AG
Gstm1 F	CTACCTTGCCCGAAAGCAC
Gstm1 R	ATGTCTGCACGGATCCTCTC
Gstm3 R	TGA AGG CCA TCC CTG AGA AA
Gstm3 F	CTT GGG AGG AAG CGG CTA CT
Gstm5 R	AGA TAC ATC GCA CGC AAG CA
Gstm5 F	CCA TGT GAA TTT CCC CAG GA
Hnf4α F	TGCCTGCCTCAAAGCCAT
Hnf4α R	CACTCAGCCCCTTGGCAT
HO-1 F	GTCAAGCACAGGGTGACAGA
HO-1 R	ATCACCTGCAGCTCCTCAAA
Il-1ϟ F	GGGCCTCAAAGGAAAGAATC
Il-1ϟ R	TACCAGTTGGGGAACTCTGC

KI67 F	AGG ATG GAA GCA AGC CAA CA
KI67 R	GGC CCT TGG CAT ACA CAA AA
Krt7 F	CACCCGGAATGAGATTGCG
Krt7 R	GCACGCTGGTTCTTCAAGGT
Krt19 F	TGCTGGATGAGCTGACTCTG
Krt19 R	AATCCACCTCCACACTGACC
Mcp1 F	TGAATGTGAAGTTGACCCGT
Mcp1 R	AGAAGTGCTTGAGGTGGTTG
Nq01 F	AGC GTT CGG TAT TAC GAT CC
Nq01 R	AGT ACA ATC AGG GCT CTT CTC G
Nrf2 F	TTC TTT CAG CAG CAT CCT CTC CAC
Nrf2 R	ACA GCC TTC AAT AGT CCC GTC CAG
Oga F	TTCACTGAAGGCTAATGGCTCCCG
Oga R	TGTCACAGGCTCCGACCAAGT
Ogt F	TCGCACAGCTCTGTCAAAAA
Ogt R	GCCCTGGGTCGCTTGGAAGA
Phgdh F	GGAGGAGATCTGGCCTCTCT
Phgdh R	GCACACCTTTCTTGCACTGA
αSma F	TGA CCC AGA TTA TGT TTG AGA CC
αSma R	CCA GAG TCC AGC ACA ATA CCA
Tbp F	CCCCACAACTCTTCCATTCT
Tbp R	GCAGGAGTGATAGGGGTCAT
Tgfβ F	TGAGTGGCTGTCTTTTGACG
Tgfβ R	AGTGAGCGCTGAATCGAAAG
Tnfα F	TGGGAGTAGACAAGGTACAACC
Tnfα R	CATCTTCTCAAAATTCGAGTGAC